

TEET KUUTMA

Galaxies and non-galactic baryons
in cosmic filaments



DISSERTATIONES ASTRONOMIAE UNIVERSITATIS TARTUENSIS

23

TEET KUUTMA

Galaxies and non-galactic baryons
in cosmic filaments



UNIVERSITY OF TARTU
Press

This study was carried out at Tartu Observatory, University of Tartu, Estonia.

The Dissertation was admitted on September 16 2021, in partial fulfillment of the requirements for the degree of Doctor of Philosophy in physics, and allowed for defense by the Council of the Institute of Physics, University of Tartu.

Supervisor: Dr. Antti Tamm,
Tartu Observatory, University of Tartu,
Tõravere, Estonia

Opponent: Dr. Pasi Nurmi,
Department of Physics and Astronomy, University of Turku,
Turku, Finland

Defense: November 4, 2021, Tartu Observatory, University of Tartu, Estonia

ISSN 1406-0302

ISBN 978-9949-03-713-1 (print)

ISBN 978-9949-03-714-8 (pdf)

Copyright Teet Kuutma, 2021

University of Tartu press

www.tyk.ee

CONTENTS

List of original publications	7
List of acronyms and terms used	8
Introduction	9
1 Background	13
1.1 Large-scale structure formation	13
1.1.1 Observations	14
1.1.2 Numerical simulations	15
1.2 Cosmic filaments	17
1.3 Galaxy evolution	19
2 Role of filaments in galaxy evolution	21
2.1 Theoretical considerations	21
2.2 The filament environment in observations	22
2.2.1 Brightest group galaxies (BGGs)	24
2.3 The intergalactic medium	25
2.4 Alignment studies	25
2.5 Specific questions addressed in this thesis	26
3 Data and methods	27
3.1 SDSS – Sloan Digital Sky Survey	27
3.2 The Evolution and Assembly of GaLaxies and their Environ- ments (EAGLE) simulation	29
3.3 Bisous filament finder	30
3.4 Luminosity density field	33
3.5 Galaxy and filament selection	35
3.5.1 Specifics in Paper I	35
3.5.2 Specifics in Paper II	36
3.5.3 Specifics in Paper III	38
3.6 Statistical comparison of SDSS and EAGLE galaxies	38
3.6.1 Galaxy number density	40
3.6.2 Luminosity and mass functions	43
4 Results	45
4.1 Properties of galaxies in filaments.	45
4.2 Group properties and brightest group galaxies in filaments.	49
4.3 Intergalactic diffuse gas in filaments	51
5 Discussion and conclusions	54

References	57
Summary in Estonian	66
Acknowledgements	69
Attached original publications	71
Curriculum vitae	117
Elulookirjeldus	121

LIST OF ORIGINAL PUBLICATIONS

This thesis is based on the following publications:

- I **Kuutma, T.**, Tamm, A., & Tempel, E. 2017, *From voids to filaments: environmental transformations of galaxies in the SDSS*, *Astronomy & Astrophysics*, 600, L6
- II **Kuutma, T.**, Poudel, A., Einasto, M., Heinämäki, P., Lietzen, H., Tamm, A., & Tempel, E. 2020, *Properties of brightest group galaxies in cosmic web filaments*, *Astronomy & Astrophysics*, 639, A71
- III Tuominen, T., Nevalainen, J., Tempel, E., **Kuutma, T.**, Wijers, N., Schaye, J., Heinämäki, P., Bonamente, M., & Ganeshaiyah Veena, P. 2017, *An EAGLE view of the missing baryons*, *Astronomy & Astrophysics*, 646, A156

Author's contribution to the publications

The Author has made considerable contributions to the following original publications. The following list gives details on the author's work in each of the papers. The Roman numerals correspond to those in the list of publications.

Publication I. The author selected the galaxies and filaments from catalogues, analysed the data, wrote the text of the paper and prepared the figures.

Publication II. The author prepared the galaxy catalogue for the filament finder and analysed the resulting data. He wrote most of the text and prepared most of the figures.

Publication III. The author was significantly involved in the development of the methodology of observational traces of WHIM. He prepared some figures and wrote some of the text.

LIST OF ACRONYMS AND TERMS USED

BGG - brightest group galaxy

DM - dark matter

EAGLE - Evolution and Assembly of GaLaxies and their Environments simulation

H_0 - Hubble constant

HAM - Halo Abundance Matching

H_I - neutrally charged hydrogen

LDF - luminosity density field

LSS - large-scale structure

Mpc - megaparsec, 10^6 parsecs

M_r - absolute luminosity in r -band

M_* - stellar mass

M_\odot - mass of the Sun

NUV - near ultra-violet

SDSS - Sloan Digital Sky Survey

SSFR - specific star formation rate, the star formation rate normalised by stellar mass

WHIM - warm-hot intergalactic medium

z - cosmological redshift

Λ CDM - concordance cosmology with a cosmological constant and cold dark matter

Å - angstrom, 10^{-10} metres

INTRODUCTION

Galaxies are some of the most eye-catching objects observable in the night sky. Due to their distance however, only a handful can be observed without the use of telescopes: the disk of our own Milky Way galaxy, the core of our largest neighbouring galaxy (Andromeda), and the two Magellanic Clouds, which are irregularly shaped satellites of the Milky Way. Even these few are faint enough to need a moonless, dark sky to see. Since the invention of the telescope, sky studies have shown the universe to be filled with galaxies. At first they were assumed to be nebulae within our own galaxy, but since the early 20-th century, when their distances were first measured, they were identified as other collections of stars like our own galaxy.

The basis of galaxy evolution is the change in its constituent stars. Stars provide the visible light which allows galaxies to be observed and interact with the galaxy as a whole. In stars, gas is transformed into elements heavier than hydrogen and helium, which enrich the universe with chemicals that are released into the void when stars meet their explosive end. Gas clouds coalesce and form new stars with different chemical compositions and the cycle continues. The processes of gas enrichment and deprivation, driven by energetic stellar phenomena and galaxy interactions over cosmic time, determine many galaxy properties.

There is a varied zoo of galaxies with a variety of sizes and shapes. The most prominent features of galaxies are a centrally concentrated bulge and a flattened disk, with most large galaxies containing one or both components. In the simplest terms, galaxies show how such a large amount of matter behaves under its own gravity. However, there are many more interactions at work that give galaxies the breadth of appearances observed. How galaxies evolve to have their current varied properties is a subject of ongoing research in astrophysics.

Looking beyond galaxies towards the larger scale, in the cosmos, matter tends to combine, as a consequence of physical forces, into structures that themselves form parts of larger structures. A planet is part of a solar system dominated by one or more stars. These stars form a part of system of stars, either a galaxy or a star cluster within a galaxy. Galaxies also form part of a larger structure, the large-scale structure (LSS).

Indeed galaxies are distributed not randomly, but in preferred configurations. The most visible are dense knots consisting of hundreds to thousands of tightly clustered galaxies. These are contrasted by sparse voids containing few or no galaxies, which constitute most of the volume of the universe. Voids are surrounded by walls which are difficult to discern because they contain few galaxies. Sparser than knots, but denser than voids and walls, there are also fil-

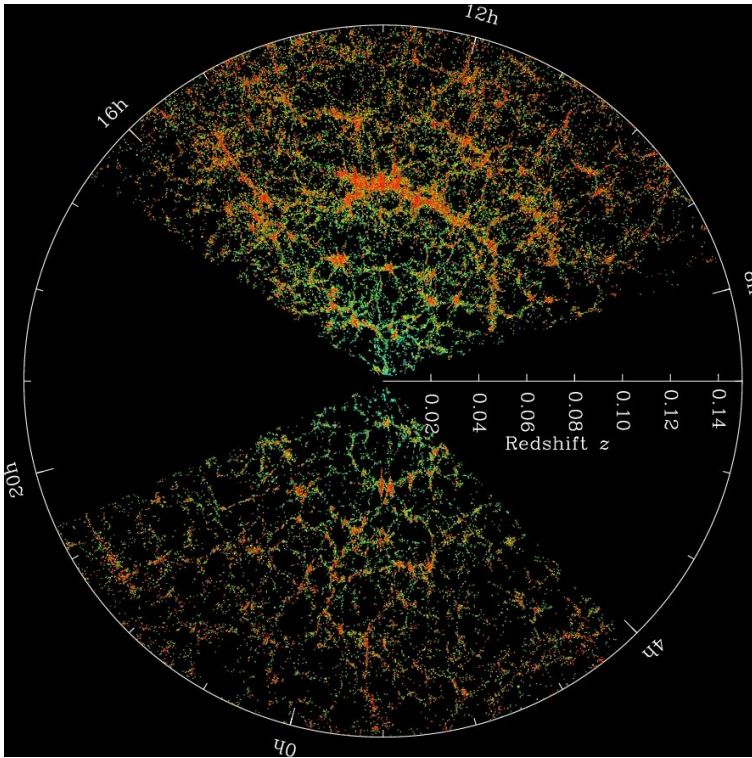


Figure 1: The SDSS map of the universe. Each dot is a galaxy; the colour is the $g - r$ colour of that galaxy. The LSS components are discernible in the galaxy distribution. Image Credit: M. Blanton and SDSS (<https://www.sdss.org/>).

aments, which are chains of galaxies only a few megaparsecs (Mpc) in diameter, but which extend from a few to tens of Mpc long. The most prominent and largest filaments form bridges between the knots. In Figure 1 the distribution of galaxies in the nearby universe is shown shows with visible knots, filaments, and voids. From the locations of galaxies alone, walls are difficult to discern. The interconnected network of knots, filaments, and walls surrounding voids have come to be called the cosmic web. In the current concordance Λ CDM cosmological model, the LSS forms from an almost smooth initial matter distribution through the effect of gravitational interaction (e.g Zel'dovich 1970; Bond et al. 1996).

From stellar velocity measurements, it seems that stars in galaxies move too fast for the visible matter to keep them in their orbits. This tendency extends to galaxies that move inside groups and clusters. Beyond the baryonic matter of which stars and gas consist of, there has to be more matter in and around galaxies that is not observed. Because of its mysterious nature, this matter component is called dark matter (DM). The exact nature of DM is still unclear. The only observed interaction it has with visible matter is through

gravity. Observations have shown that every galaxy is surrounded by a DM halo, several times more massive than the baryonic matter content. It is evident that through its gravitational impact, the DM component forms the backbone of the LSS, in which galaxies are a visual trace of the underlying matter distribution. Thus, study of the LSS can lead to a better understanding of the nature of DM.

Are galaxies in different cosmic web environments also different? Early studies already found that galaxies in knots compared to those in voids are more elliptical and redder (Dressler 1980). These morphological changes hint that the environment has a role in shaping galaxies. Galaxy evolution is modified to a large part due to interactions; that is, in environments where galaxies are closer together there are more galaxy–galaxy interactions. Besides galaxies, a significant part of baryons is in the form of diffuse gases located outside the gravity wells of haloes. This matter is difficult to detect, but can play an important role in galaxy evolution as it is expected to reside within the structures of the cosmic web.

In recent years, several methods of detecting cosmic web structures have been developed. Knots and voids have been studied for decades due to being easier to detect based on relatively simple metrics like galaxy counts. This is not the case for filaments and walls, which are not isotropic and require a more rigorous computational framework to be detected. Some current methods for finding cosmic web components need detailed phase-space information, making them currently better suited for large-scale structure simulations rather than observations. Only a few methods have been developed that are designed to be explicitly applicable to observed data. Over the past decades, galaxy redshift surveys have become ever larger in depth and volume, enabling statistical studies of large numbers of galaxies in a variety of cosmic regions. These developments open up the possibility to gain new insights into galaxy evolution in the context of cosmic web structures.

The project presented in this thesis was set up with the goal of understanding the connection between baryonic matter and the cosmic web. Specifically, the focus is on cosmic web filaments and to what extent the filament environment affects the properties of galaxies and diffuse baryons within filaments. To answer this question we gathered data on the properties of galaxies from the Sloan Digital Sky Survey (SDSS). Filaments were extracted from the galaxy distribution using the Bisous filament finder. The emphasis was on disentangling filament effects from other known galaxy–environment correlations. The impact of the filament environment on the intergalactic medium is even less well understood. The intergalactic medium is expected to be concentrated along filaments. However it is too diffuse to detect all of it with current telescopes. Because of this, a hydrodynamic simulation, EAGLE, was used here to study diffuse baryons in filaments.

The thesis is summarised as follows: Chapter 1 gives more detailed back-

ground to the large-scale structure, galaxies and terminology involved. The question of baryon–filament interaction is discussed in chapter 2 along with other studies on this subject. In chapter 3, the data and the analytical methodology is presented. The results of the published articles connected to this thesis are presented in chapter 4, and in chapter 5, an interpretation of the results in the context of wider research and the conclusions of this thesis are made.

CHAPTER 1

BACKGROUND

1.1 Large-scale structure formation

The formation of DM haloes in which galaxies form in the Λ CDM model has been thoroughly studied (Peebles 1980; Frenk & White 2012). Below is a brief description of the process from the initial density field to observable galaxies. The initial matter configuration is a distribution with a globally smooth density profile with small gaussian perturbations in an expanding background. Matter condenses in the high density peaks of the perturbations. Haloes form when the overdensity becomes high enough to overcome the background expansion. Structure formation is hierarchical, meaning that low mass haloes form first, which merge to form larger haloes. Baryons gather and cool inside collapsed haloes forming galaxies. Importantly the galaxies observed today carry information on their formation history. More massive systems have had more chances to grow through merging, while less massive galaxies either formed later or evolved in seclusion. Another reflection of this process is that the small perturbations in the primordial density field evolved into the peak-void structure observed in galaxy distribution in the local universe (van de Weygaert & Bond 2008).

As structures evolve, density contrast increases and anisotropic effects start to play a role in further clustering of matter. Small deviations from spherical geometries are enhanced by gravity, leading to anisotropic structures. This property is intrinsic for a gravitational force in a random density field (Bond et al. 1996). The anisotropic collapse manifests in the formation of filamentary and wall-like structures. The knots, which arose from the primordial density field peaks, grow at the crossing of the filaments. The voids, delineated by walls, grow with the background expansion of the universe, while matter is drained out of them towards higher density regions due to gravitational attraction.

The formation of different structures can be understood through the Zel'dovich formalism (Zel'dovich 1970). If the tidal deformation effect is projected along three axes, then different structures form depending along which axes the collapse is fastest. Collapse along one axis forms flattened walls, along two axes elongated filaments, and along three axes spherical knots. The collapse is fastest along one axis at a time, with walls forming first, filaments inside walls and finally clusters at the end-points of filaments.

The matter budget in the universe is dominated by non-luminous DM. This was established nearly a century ago by Zwicky (1933, in German), see Frenk & White (2012) for a recent review in English. According to current estimates,

DM outweighs baryons five to one (Planck Collaboration et al. 2020). The first haloes that formed in the early universe had to be made of DM as they are more massive and immune to effects of internal pressure, which can slow collapse. Thus the distribution of luminous galaxies is a visual trace of the underlying DM distribution many times more massive than the galaxies themselves.

DM can only be measured indirectly as it does not radiate in the electromagnetic spectrum and interacts with baryons only through gravity. Several methods of measuring DM components of galaxies and galaxy groups have been devised. DM halo masses can be estimated from stellar velocity dispersions of stars in galaxies according to the virial theorem of relaxed self-gravitating systems. This method has been used to measure group and cluster masses based on the velocities of galaxies in those systems. Lensing studies probe DM through the deformation of more distant galaxies by a nearby 'lensing' galaxy along the same line of sight.

The model described above is the result of decades of research and has observational and theoretical support from a variety of studies. Below is a summary of how the LSS is studied, with an emphasis on observational surveys and cosmological simulations.

1.1.1 Observations

LSS components can span large areas on the sky; for example cosmic filaments can be several degrees in length on the sky, making direct observation of the LSS complicated. Specific observing strategies need to be used to map the the largest structures on the sky.

The most important observational probes of cosmic structures are large-scale redshift surveys, with the goal of accurately mapping positions of objects in the sky. For galaxies, redshift measurements allow the mapping of their positions in three dimensions. The resulting 3D maps of the universe contain a wealth of data for a number of fields of research, from stellar physics to cosmology. Some of the most prominent surveys from the past decades are the Sloan Digital Sky Survey (SDSS, York et al. 2000), the 2-degree Field Galaxy Redshift Survey (Colless et al. 2003), the Two Micron All Sky Survey (Huchra et al. 2005), and the Galaxy And Mass Assembly (Driver et al. 2011).

Already in early galaxy redshift surveys Jöeveer & Einasto (e.g. 1978), the components of the cosmic web were identified. Knots and voids were identified first due to their large density contrast, while filaments, and especially walls, were difficult to identify. The components of the cosmic web are interconnected without sharp edges delineating the separate components. Their exact definitions are subjects of ongoing research. While discernible to the human eye, filaments are difficult to constrain computationally, as the components of the LSS can appear on different scales due to hierarchical clustering. The limited spatial coverage of the full LSS from observed galaxies and the

difficulty of determining the velocity information of cosmic flows complicates the process of accurately determining these dynamically evolving LSS components.

In observations, the vast distances to galaxies set a limit on how faint a target can be observed. With increasing distance, progressively brighter galaxies fall out of the visibility of a survey as they become indistinguishable from the background noise in taken images. This can be compensated for with larger telescopes, more sensitive cameras and longer exposure times; however all of these also increase the cost of any given survey.

In galaxy surveys, nearby galaxies also pose a problem. Most surveys cover only the part of the sky that is observable from the survey site. If the volume of a survey that is contiguous on the sky is visualised in three dimensions it forms a cone shape. The observer is situated at the tip of that cone with space near the observer covering a small volume of the entire survey. While fainter galaxies would be easier to detect nearby, the total number of galaxies is insufficient for estimation of the size and types of large-scale structure elements here. This essentially sets a lower limit to LSS studies, which depends on the sky area covered in different surveys.

Additional considerations in observational studies include measurement accuracies of photometric and spectroscopic instruments and the algorithms used to convert measured light into physical parameters. These contribute to errors in the measured and derived parameters of galaxies. The advantage of surveys as a means to overcome this is that they enable sampling of a large numbers of galaxies. Large samples can overcome non-systematic errors by accounting for variation in the data.

1.1.2 Numerical simulations

The physics involved in evolution of the LSS has proven to be too complex for analytical calculation. Numerical simulations are needed to gain detailed insight into the formation and evolution of the LSS and the galaxies therein. Additionally, in sky surveys it is impossible to observe the evolution of individual cosmic structures. The time scales over which these structures evolve stretches from millions to billions of years. Simulations allow modelling of the evolution of individual galaxies, groups or several LSS components over the full range of cosmic time. N-body simulations have been able to reproduce the observed cosmic web in increasing detail (e.g. Gramann 1993; Springel et al. 2005; Cautun et al. 2014).

The most advanced simulation algorithms allow us to follow the evolution of matter from the nearly flat initial conditions to the large Mpc-scale structures observed today. The simulations can be categorised as dark matter only and hydrodynamical. N-body simulations ignore baryon interactions and are used to model the evolution of dark matter through gravitational effects. Hydrody-

namical simulations model the baryons in addition to dark matter, including such processes as stellar evolution, feedback and gas dynamics. These are computationally more complex and, as a result, hydrodynamical simulations cover smaller volumes compared to N-body simulations. Vogelsberger et al. (2020) gives a review of recent cosmological numerical simulations. Current simulations contain volumes ranging from a few tens of cubic Mpc for zoom-in simulations to several thousand cubic Mpc for the largest N-body simulations. Zoom-in simulations are designed to study the evolution of individual galaxies.

While in cosmological simulations the Mpc scales at which LSS forms can be observed, the physics occurring on smaller scales is not possible to calculate because of the vast difference in scales involved. The workaround has been to model these smaller-scale processes using sub-grid recipes, accounting for processes such as star formation, black hole growth, supernovae feedback, and stellar winds by bulk summation over stellar populations. These processes have to be tuned based on observational studies.

In hydrodynamical simulations the data is perfect in the sense that all galaxies are detected and have parameters without measurement errors. However, there are important shortcomings that have to be considered. Firstly, the galaxies that are formed in simulations depend on the initial conditions, the cosmological parameters and the algorithmic mechanisms governing galaxy evolution in the simulation. With the goal being to form simulated galaxies similar to observed galaxies, the physics governing galaxy formation has to be approximated as close as possible to real physics in the simulation algorithms. Of course the physical processes governing galaxy evolution are still under research, with simulations themselves being an important tool in unravelling this complicated problem. Thus, an iterative process forms, with previous simulations forming the theoretical understanding leading to more advanced simulations.

Another aspect of simulations is resolution effects. These effects appear in the time parameter since computational limitations make it unreasonable to run a simulation consisting of millions or billions of particles such that the exact motions of all these particles are calculated at any required time. The workaround is to calculate particle positions and motions at regular time intervals, called snapshots. Each snapshot is a record of all particle parameters and acts as a starting point for calculating the next snapshot.

Besides the time dimension, resolution effects also affect spatial properties of cosmological simulations. Simulations usually consist of a set number of particles. The scale that a simulation covers is tuned by the distance over which particle–particle interactions are calculated. This means that different simulations containing the same number of particles can cover the space around a single galaxy and its nearby volume of space or a significant part of the universe containing many thousands of galaxies. While it would be desirable to simulate as large a fraction of the universe as possible, in such a case there

would be a limited number of particles forming each individual galaxy. The number of particles a galaxy consists of affects how accurately the properties of those galaxies can be calculated.

1.2 Cosmic filaments

Filaments represent a typical environment for galaxies, as about half of galaxies and 40% of the mass in the universe are located within them (Aragón-Calvo et al. 2010). Filamentary structures can be identified on a large range of scales, from elongated superclusters (Porter & Raychaudhury 2005) to tenuous tendrils within voids (Crone Odekon et al. 2018). Numerous studies have found filaments to be fractal in nature (Aragón-Calvo et al. 2010; Sousbie et al. 2011; Einasto et al. 2012; Alpaslan et al. 2014; Darvish et al. 2017; Malavasi et al. 2017). Based on DM simulations, filaments are typically found in regions of density several times the cosmic average and vary in length from a few up to around 100 Mpc (Cautun et al. 2014). Accordingly, median diameters change from one to four Mpc, with longer filaments also being thicker. In observations, filament properties vary based on the detecting algorithm. Rost et al. (2019) compared three finding algorithms on SDSS galaxies. They found filaments with maximum lengths between 15 and 40 Mpc, with the bulk of filaments in the 5-10 Mpc range.

Figure 1.1 shows spatial distribution of simulated filaments of different sizes. Larger filaments are wider and contain many haloes and galaxies, with massive clusters forming the endpoints of filaments. The smallest filaments are only sparsely traced by haloes in low density environments, possibly forming inside voids. Three examples of walls are shown in the figure.

Observations of prominent filaments (Giovanelli et al. 1986; Ebeling et al. 2004; Porter & Raychaudhury 2005) and numerical simulations (Colberg et al. 2005; Benítez-Llambay et al. 2013; Cautun et al. 2014; Tempel et al. 2014a) indicate the dynamical nature of filaments, characterised by matter flows from less dense environments, like voids and walls towards knots. This implies that in filaments beyond density contrast there is expected to be a directed velocity field that channels baryons along its orientation. Based on density alone, the filament environment represents an intermediate medium between voids and clusters with significant density overlap between filaments and other environments.

Baryonic matter outside of galaxies is another consideration. Estimates from galaxy surveys determine the amount of baryonic matter in galaxies, groups, and clusters to be in the order of 10–20% of the total baryonic content (Fukugita & Peebles 2004). Thus, most of the baryonic matter in the local universe resides in the intergalactic medium. This matter component is composed mainly of the primordial gas not yet accreted into galaxies. The intergalactic medium moves along cosmic flows in the different LSS components. Fila-

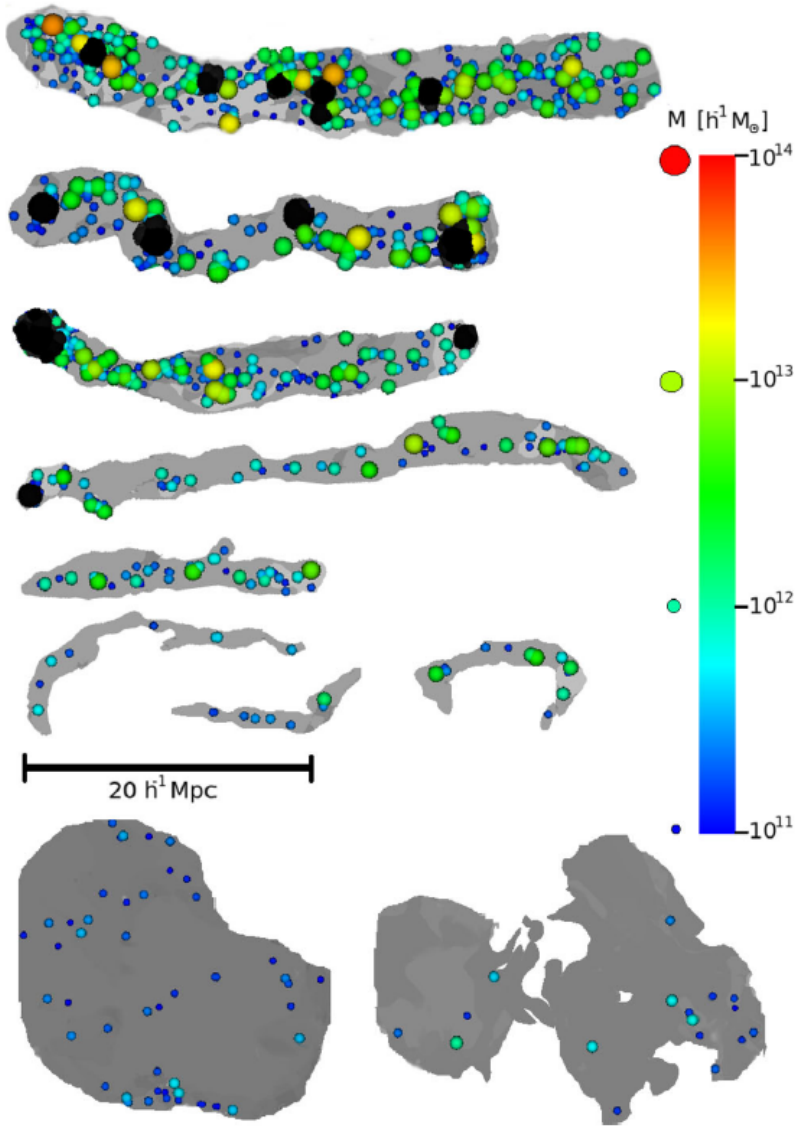


Figure 1.1: Examples of filaments and walls in the Millennium N-body DM simulation. LSS structures were extracted using the NEXUS+ algorithm. Original caption: The population of haloes in a few typical filaments (top rows) and walls (bottom-most row). Haloes are shown via points whose size and colour depends on the halo mass as shown in the right-hand legend. For filaments, the black points show haloes found in cluster regions. The length-scale of the objects is shown via the horizontal bar on top of the last row of graphs. Source: Cautun et al. (2014).

ments contain a large portion of these baryons, but not all of this matter has been firmly detected yet.

1.3 Galaxy evolution

Galaxies form the primary observational source of information about the evolution of cosmic structures and the backbone of all observational studies about the larger universe. They are the sites of chemical evolution driven by stars, which causes both the chemical transformation of primordial hydrogen–helium gas into heavier elements and creates the light that makes cosmic structures observable. Besides stars, galaxies contain black holes, gas and dust, all of which change and interact over time, contributing to the overall evolution of the galaxy.

Properties of galaxies depend largely on the stellar mass (Kauffmann et al. 2003). Massive galaxies tend to have less star formation, and be redder and bulge-dominated. This mass-dependence implies that over time, as galaxies deplete their gas content, their stellar populations undergo associated changes, referred to as ageing. However galaxies do not evolve in seclusion, but with effects from external factors that affect their evolution as well. With increasing environment density, galaxy interactions, like mergers between similarly sized galaxies, and cannibalism, where a larger galaxy absorbs a smaller one, are increasingly likely to occur. These interactions are a natural continuation of the hierarchical matter clustering discussed in the previous chapter. They can have profound effects on properties of galaxies. Below some correlations between galaxies and their environments are summarised .

The morphology–density relation implies that galaxies in denser environments are preferentially of earlier types, more massive, and more passive (Hubble & Humason 1931; Zwicky 1938; Dressler 1980; Postman & Geller 1984; Kauffmann et al. 2004; Gómez et al. 2003). This relation is the result of the combination of several effects. One factor is the initial birthplace of galaxies and their surrounding haloes. Locations where the primordial density was higher at the beginning accumulate more mass faster. As a result, galaxies at these locations form earlier and evolve faster reaching a more evolved state (elliptical morphology, gas-poor, low star-forming activity) sooner. Another factor is the proximity of a galaxy to galaxy clusters. Studies have shown that galaxies falling into clusters experience effects that strip them of their star-forming gas. This includes ram-pressure stripping (Gunn & Gott 1972) and interaction with the cluster potential (Hwang et al. 2018). Opposed to these effects is galactic cannibalism, which enriches the larger galaxy with new supplies of star-forming gas (Gunn & Gott 1972; Moore et al. 1996; Peng et al. 2010). A correlation has been observed between masses of galaxies and the density of the environment (Oemler 1974; Kaiser 1984), which is, in effect, similar to the morphology–density relation.

Another aspect is ‘galaxy conformity’, an observation showing that galaxy SSFRs are strongly dependent on the SSFRs of their nearest massive neighbours (e.g. Weinmann et al. 2006; Park et al. 2007; Kauffmann et al. 2013; Hearin et al. 2016). This has been observed for galaxies in the same group (one-halo conformity) and galaxies in different haloes, up to separations of 4 Mpc (two-halo conformity). The cause of this is likely to be the large-scale structure - that is, haloes in similar large-scale environments are likely to have correlating merging histories, leading to similar observed properties.

CHAPTER 2

ROLE OF FILAMENTS IN GALAXY EVOLUTION

Mass and local density are important drivers of galaxy evolution (e.g. Balogh et al. 2004; Baldry et al. 2006). The large-scale environment, especially knots, also affects galaxy evolution, as evidenced by different clustering-related effects. Filaments represent a typical environment for galaxies and baryonic matter in general (Aragón-Calvo et al. 2010). Therefore, it is important to ask to what extent the filament environment affects galaxy evolution. Below, some studies that probe the interactions between galaxies, their haloes, and the cosmic web, all in the context of filaments, are discussed.

While filaments contain a large portion of all matter in the universe, not all of it is in galaxies. Studies of the matter budget have found that galaxies and galaxy groups contain only up to a fifth of the baryon budget (Shull et al. 2012). The rest of the baryonic matter is in the form of diffuse gases located, like galaxies, within cosmic web structures. The extent and the method of interaction between galaxies and diffuse material is still under study from several viewpoints.

2.1 Theoretical considerations

A recent study by Aragon Calvo et al. (2019) contextualises the quenching of galaxies in cosmic web structures, specifically filaments, as a Cosmic web detachment model. Zoom-in simulations of galaxy formation have shown that in the early universe, galaxies accrete gas from the environment through primordial fiducial filaments. The theory posits that as a galaxy enters a filament (or a wall or a knot), non-linear interactions destroy the fiducial channels, stripping the galaxy of the source of its star-forming gas, bringing about an eventual quenching.

Recent works have looked at the filament as a transport pathway towards knots. In this picture, the filament forms a two-way channel with cosmic flows along the filament pointing towards the nearest knot. In the midway region along the filament, a saddle forms. Musso et al. (2018) took an analytical approach using excursion set theory to derive mass accretion rates of haloes depending on their perpendicular distance to filaments and distance from saddle points along filaments. Kraljic et al. (2019) used simulated data and stacking of multiple filaments to detect mass and SSFR gradients along the filament both as a function of distance from the saddle and distance from the filament spine.

Several hydrodynamical simulations have found evidence of cold gas inflows into the centres of DM haloes in preferred directions (Kereš et al. 2005;

Dekel et al. 2009; Pichon et al. 2011). Cold gas, in cosmological terms gas at a temperature of $T < 10^5 K$, is important as it can condense into the star-forming disks of galaxies, leading to sustained star formation. At the same time, inflows in preferred directions build up angular momentum in galaxies, which leads to preferred alignments along cosmic filaments (see chapter 2.4 below).

In recent years, another method of measuring the impact of large-scale structure on galaxies and their haloes has formed called connectivity (Codis et al. 2018). These authors determined a correlation between properties of galaxy clusters and the number of filaments connected to the clusters. Clusters with more connectivity are, on average, more massive and contain fewer active galaxies (Kraljic et al. 2020). Darragh Ford et al. (2019) found that the mass of group-central galaxies correlates with connectivity in low-mass groups, while for high-mass groups there is anticorrelation.

2.2 The filament environment in observations

In recent years, several studies have looked at filaments as distinct galaxy environments. Studies have identified some prominent individual filamentary structures connected to clusters of galaxies, but also filaments in less dense environments with filament finder algorithms. Below, some publications that have looked at properties of galaxies in filaments are discussed.

Studies of prominent individual filamentary structures show differences in filament galaxies compared to cluster and field environments. Fadda et al. (2008) reported two filamentary structures on the outskirts of cluster Abell 1770, discovered using the Spitzer infrared space telescope (Werner et al. 2004). The filament galaxies have higher SFR compared to the cluster. Biviano et al. (2011) looked at cluster Abell 1763, which contains a filament connecting to the cluster core. They found a higher number of infra-red-emitting galaxies in the filament compared to the cluster core and cluster outskirts. Darvish et al. (2014) used the Multi-scale Morphology Filter (Aragón-Calvo et al. 2007) in the COSMOS field at $z = 0.84$, identifying galaxies in different Cosmic Web structures. They found that the fraction of $H\alpha$ -emitting galaxies is enhanced in filaments compared to clusters and the field. This implies an increase in star-forming galaxies in filaments at that redshift. Darvish et al. (2015) studied a filament with 28 star-forming galaxies in the COSMOS field at $z = 0.53$. They found filament galaxies to be more metal enriched and to have significantly lower electron densities. They speculate a longer star-formation time scale for filament galaxies. The filaments in these studies are in or near cluster environments, which are already overdense regions. In addition, these studies only look at a few filaments. Considering these limitations, it is difficult to draw conclusions about the entire filament environment based on these studies alone.

Several studies have found changes in galaxy properties with respect to the locations of galaxies within filaments. The largest gradients are observed based on the distances of galaxies to filament spines. Alpaslan et al. (2016) studied stellar mass and star-formation rate (SFR) of isolated spiral galaxies in the GAMA Survey as a function of filament distance up to $z \leq 0.09$. They found that stellar mass increases towards the filament axis, while at fixed mass, SSFR decreases. They determined that even though stellar mass is the primary determinant in star formation activity, the large-scale environment imprints a secondary effect. They also suggested that gas accretion from voids onto filaments happens in a primarily orthogonal direction. Chen et al. (2017) used SDSS DR12 and The Cosmic Web Reconstruction catalogue (Chen et al. 2016) to determine filament effects on galaxies up to redshift $z = 0.7$. They found filaments to have similar effects on $z = 0.7$ galaxies as clusters: more massive and redder galaxies to be closer to filament axes. Malavasi et al. (2017) studied VIPERS galaxies at redshift $z \sim 0.7$. They found more massive and passive galaxies on filament axes. Similarly Kraljic et al. (2018) found galaxies in the GAMA survey at distances in the range $0.03 < z < 0.25$ to be more massive and passive closer to axes. They also noted a correlated reddening in dust-corrected $u - r$ colour. Laigle et al. (2018) studied COSMOS2015 catalogue galaxies and compared their results to Horizon-AGN simulated galaxies. They used 2D filaments that closely matched 3D data. The data covered distances in the range $0.5 < z < 0.9$. They found massive galaxies to be statistically closer to filaments. At fixed stellar masses, passive galaxies were also shown to be closer to filaments. They demonstrated that the signal persists after accounting for effects of nodes and local density. Salerno et al. (2019) found evidence of colour-determined ($NUV - r$ versus $r - K$) quenching in filament galaxies in the redshift range $0.43 < z < 0.89$ of VIPERS galaxies. They determined that stellar mass is the main factor in quenching. The results of these publications indicated a general trend for galaxies in filaments to be more massive, redder and less star forming. Also the filament-based effects are second order – that is, the signal of filament effects on galaxies is small. Thus, large samples of galaxies within and outside filaments need to be compared.

How the shape of filaments may affect galaxies is less studied. Shim et al. (2015) found a correlation between the straightness of void filaments and the luminosity of galaxies within them. This result implies that the efficiency of gas transportation from the surrounding void into galaxies is enhanced in straight filaments.

Besides stellar properties H_I gas plays an important role in galaxy evolution. Stars form from dense H_I clouds inside galaxies and star formation is strongly correlated with the presence of H_I gas (Kennicutt 1998; Catinella et al. 2013). In relation to filaments Crone Odekon et al. (2018), found the H_I content of galaxies to decrease closer to filament spines. They found the most H_I -rich galaxies inside voids in smaller 'tendrils' filaments.

In contrast, several studies have found that the local, group-scale environment is the only driver of galaxy properties. The counter-argument is that the larger-scale filament environment only forms a density enhancement from which the observed changes in galaxies are measured. Yan et al. (2013) calculated the tidal environment of SDSS DR7 galaxies. They estimated the tidal field based on the smoothed spatial number density of galaxies and on the ellipticity of the potential field derived from the tidal field. They found density to be the main determining factor of the colours, amplitude of the 4000 Å break, concentration, and size of galaxies. Eardley et al. (2015) used GAMA and the tidal tensor prescription, based on the Hessian of the pseudo-gravitational potential, to detect large-scale environment knots, filaments, walls, and voids. They looked at luminosity functions of galaxies in different environments and attributed changes solely to the local-density dependence. Brouwer et al. (2016) combined overlapping GAMA and KiDS data to measure halo masses based on galaxy–galaxy lensing. They found no dependence of the average halo mass of central galaxies on their cosmic web environment. They only noted a change in halo mass that can be completely attributed to the local density of galaxies. Goh et al. (2019) found, in simulation data, that at fixed environmental densities, the cosmic web does not affect dark matter halo properties: specific mass accretion rate, spin parameter, concentration, prolateness, scale factor of the last major merger, and scale factor when the halo had half of its present day mass.

2.2.1 Brightest group galaxies (BGGs)

In addition to the connection between filaments and galaxies in general, it is of importance to consider different sub-populations of galaxies. In groups and clusters, one galaxy tends to dominate the environment, being located centrally in the group (Lange et al. 2018) and being brighter and more massive than other group members (satellite galaxies). Galaxies without satellites are referred to as isolated.

The brightest group galaxies (BGGs) evolve differently to other group members, having shorter star-formation timelines (Von Der Linden et al. 2007). Shen et al. (2014) determined that, on average, BGGs are 20% more massive than other group members, with differences increasing with the magnitude gap between the brightest and second brightest galaxies. BGGs are a better marker for the group environment as a whole, as the satellites are affected by the group BGG. Additionally, due to their intrinsic brightness, they are more likely to be observed in sky surveys.

While evidence of LSS impact on BGGs has been found (e.g Einasto et al. 2011; Luparello et al. 2015), the effects of the filament environment specifically on BGGs has not been thoroughly investigated. Poudel et al. (2017) showed that BGGs in filaments tend to be more massive and redder at fixed

group mass and fixed large-scale (supercluster–void) environment. Li & Chen (2019) theorised on the possibility of BGG formation, in part through cold gas accretion instead of galaxy–galaxy interactions. This would suggest the influence of filaments as a transport mechanism for the cold gas.

2.3 The intergalactic medium

Several studies have found a significant portion of the baryons in the local universe to remain undetected. This has been confirmed with simulations (Cen & Ostriker 1999; Cui et al. 2012; Martizzi et al. 2019) and observations (Shull et al. 2012; Tilton et al. 2012; Danforth et al. 2016). According to these studies galaxies, galaxy groups, and clusters account for about 10–20% of the baryon budget. A further 25% is estimated to be H I gas, which is detected through absorption lines. The rest is predicted to be in a warm-hot ($\log T(\text{K}) = 5 - 7$), low-density phase in the intergalactic medium (WHIM).

As filaments are sites of matter overdensity, but cover a larger volume compared to knots, they present a likely site for the search of the missing baryons. So far the WHIM has been difficult to detect due to its diffuse distribution. WHIM detection has so far been based on metal absorption lines. According to simulations, the primordial hydrogen of the WHIM is polluted by metals expelled by galactic winds. The low temperature phase of the WHIM at $\log T(\text{K}) < 5.5$ has been detected via absorption lines in ultraviolet spectral ranges. In the hot phase, $\log T(\text{K}) > 5.5$, the element spectral lines are in the X-ray range, but the material is too diffuse to detect with current telescopes.

2.4 Alignment studies

According to the postulates of tidal torque theory (Peebles 1969; Doroshkevich 1970; White 1984), the tidal fields that shape the cosmic web into its sub-structures also build up spin in haloes and galaxies within the haloes. This happens because of a misalignment between the non-spherical protohalo, the matter that eventually collapses into the halo, and anisotropies in the surrounding environment. The collapsing protohalo builds up spin in alignment with the surrounding large-scale environment. See Jones & van de Weygaert (2009) for a review of the subject.

Several studies using simulations have shown that spins of haloes tend to align with the orientation of filaments and walls (e.g. Aragón Calvo 2007; Hahn et al. 2007; Libeskind et al. 2013; Ganeshiah Veena et al. 2018). Interestingly, low-mass haloes tend to align parallelly, while high-mass haloes align perpendicularly, to filaments. This tendency has also been noted in observational studies (e.g. Jones et al. 2010; Tempel et al. 2013; Tempel & Libeskind 2013; Hirv et al. 2017). Alignment with filaments has also been found for galaxy pairs (Tempel & Tamm 2015) and larger satellite systems (Tempel et al. 2015).

2.5 Specific questions addressed in this thesis

Mass and local environment are major factors determining the properties of galaxies. However, a complete picture of all factors governing galaxy evolution has not yet been formed in the astrophysics community. There are many factors involved in galaxy evolution, as evidenced by the rich variety in types of galaxies and their environments. By necessity, the picture of the exact nature and processes involved in galaxy evolution has to be formed piece by piece, tackling the problem from different angles with robust theoretical models supported by observational evidence.

Galaxies located in the anisotropic filament environment experience direct modification in their properties due to the large-scale environment beyond the effects of local density. This includes modification of their alignments in accordance to tidal torque theory. Additionally, there is mounting evidence of enhancement in masses, decrease in star-formation rates and morphological transformation of galaxies in filaments. However, there is some uncertainty in the latter aspect, which has not yet been exhaustively studied. Does the intergalactic gas flowing in filaments penetrate into haloes of galaxies to feed the star formation of filament galaxies directly? Alternatively, is the density enhancement in filaments the only driver of change in the properties of galaxies? How are different galaxy populations affected by the filament environment?

Galaxies form only a part of the baryonic content in filaments. Extragalactic gas plays an important role in galaxy evolution as the basic material from which galaxies form and grow. Some of the diffuse gas has not yet been observed in the local universe. Filaments are likely candidate sites for this missing matter component. As a basis for future surveys, hydrodynamical simulations are a useful tool for determining tracers of diffuse intergalactic baryons.

The main goal of this thesis is to gain insight into the evolution of large-scale structure and the matter contained within. In order to probe the filament environment and the its baryonic content, we make use of a variety of astrophysical, computational, and mathematical toolsets. In the following chapter of this thesis, we describe in detail these various components.

CHAPTER 3

DATA AND METHODS

In this section, the datasets, both observational and simulated, are described along with the filament finder algorithm and the method used to estimate the local environment of galaxies. Also described in detail are the measured galaxy-related properties and how they are derived. During our investigation, the observed and simulated datasets were compared in statistical and empirical ways, the results of which were not included in any publication. These comparisons helped devise the selection criteria for comparable samples of galaxies in filaments and are described in this chapter.

3.1 SDSS – Sloan Digital Sky Survey

Observational data are derived from galaxy catalogues of the Sloan Digital Sky Survey York et al. (SDSS, 2000). For LSS studies, the SDSS currently has the best balance between the volume covered and the depth of the exposures in a large sky survey. The full catalogue consists of over 2 million galaxies with precise positions on the sky and spectra. From these spectra, accurate redshifts have been measured. This catalogue forms a three-dimensional map of the nearby universe within a continuous volume and provides an excellent basis for environment-based studies of galaxy systems.

The SDSS has been ongoing since 2000, and so far has observed a third of the sky with multi-band photometry and spectroscopy. The data have been made available to the scientific community in a series of roughly annual data releases. The data consist of sky images and spectra supplemented with catalogues containing measurements of different classes of objects, including Solar System bodies, Milky Way stars and other galaxies.

In the current study, we used published galaxy catalogues from Data Releases 10 (DR10) and 12 (DR12). The contiguous area of the survey covering approximately 17.5% of the full sky was used. The catalogues have been additionally supplemented with data from various sources and are available and described in their accompanying papers for DR10 (Tempel et al. 2014c), and DR12 (Tempel et al. 2017).

Due to observational limitations, the number density of observed galaxies decreases with distance because only brighter galaxies are visible at greater distances. To avoid distance-based variations, volume-limited sub-selections of the flux-limited data were used for analysis. Galaxies were selected above a brightness limit together with a distance cut at which no galaxies above the limiting brightness fall outside the survey limits. The volume-limited sample is complete in the range of luminosities considered.

In the analysis of the published papers, a variety of measurable tracers of galaxy evolution were utilised. Described below, these properties can be broadly divided into directly measured and derived ones.

Directly measured properties are those gained from the SDSS photometric images and spectra and reduced by the SDSS pipeline. The total r -band luminosity was used for the determination of the luminosity density field. The r -band was chosen as it is in the centre-most of the five optical filters of the SDSS and was the filter used when determining annuli for galaxy luminosity measurements (Petrosian magnitudes and radii are described in Blanton et al. 2001). The r -band was also chosen to determine the volume-limited samples in Tempel et al. (2014c). The difference between the g -band and i -band luminosities, the $g - i$ colour, describes in general terms the stellar content of the galaxies, with lower and higher values corresponding to bluer and redder stellar populations respectively. The $u - z$ colour would be a better trace; however, these specific filters have more noise, reducing their measurement accuracy. The concentration index is defined as the ratio of Petrosian radii containing 50% and 90% of the total luminosity of the galaxy. This parameter measures whether the stars of a galaxy are more centrally concentrated or widely dispersed. The 4000 Å break (D4000) is measured directly from the spectra of galaxies as the ratio of the blue to red continuums around the 4000 Å region of the spectrum at rest frame and estimates the time since the most recent star-forming period in a galaxy, with quiescent galaxies exhibiting the largest difference (see e.g. Gorgas et al. 1999).

Further properties of galaxies can be inferred from fitting models to galaxy luminosity profiles and spectra. The following derived parameters were used: total stellar mass of the galaxies (M_*), star-formation rate (SFR), the specific star-formation rate (SSFR, the ratio of SFR/ M_*), and stellar velocity dispersion (σ_{stars}).

Stellar mass and star-formation history are derived by fitting stellar population synthesis models on the spectra of galaxies. The models account for star-formation and metal-enrichment histories and include modulation caused by attenuation in interstellar dust (Bruzual & Charlot 2003; Conroy et al. 2009). Stellar mass is an important factor in determining galaxy properties, as discussed in Chapter 1.3, and it correlates with many other galaxy properties. For the purposes of filament effects, it is important to consider the stellar mass together with the environment of galaxies. SSFR is an estimate of overall star-formation history per unit mass in a galaxy. D4000 is a tracer for only the most recent star-forming period of a galaxy.

The visual distinction of different galaxies is a useful tool in estimating their history and current evolutionary state. For example, elliptical galaxies are bulge-dominated and have old stellar populations, while most spirals have blue disks, which indicate ongoing star formation. Less common but important classifications include lenticulars (disk galaxies with quiescent stellar popula-

tions), and irregulars (often interacting galaxies, whose morphologies are covered by the aforementioned classes).

For the morphology of galaxies in the SDSS we utilised two sources with different methodologies: visual classification and a machine learning algorithm. Galaxy Zoo (Lintott et al. 2011, L11) used citizen scientists to visually determine morphologies of SDSS galaxies using cut-out images from the survey. The galaxies were broadly classified as spiral, elliptical or undetermined. Huertas-Company et al. (2011, HC11) used a machine learning algorithm with a visually determined training sample in order to determine the likelihood of each galaxy being of elliptical, lenticular, early-type spiral or late-type spiral morphology. Both methods are in broad agreement; however, the data compiled by HC11 cover more galaxies in the SDSS.

3.2 The Evolution and Assembly of GaLaxies and their Environments (EAGLE) simulation

For simulated galaxies, a dataset was needed that included hydrodynamical modelling for the complex physics and feedback processes affecting the evolution of galaxy stellar populations. At the same time, the volume of the simulation had to be large enough to contain large-scale structure elements like filaments.

The EAGLE simulation (Crain et al. 2015; Schaye et al. 2015) is a set of hydrodynamical simulations in the framework of the concordance Λ CDM cosmology. The simulations were run in periodic cubes of 25, 50, and 100 comoving Mpc (cMpc) per side. A modified version of the Gadget-3 Smoothed Particle Hydrodynamics code (Springel 2005) was used including a series of sub-grid models for implementing sub-grid physics. Stellar feedback models were calibrated to the observed galaxy stellar mass function and galaxy sizes at the present time. The hydrodynamic particles were classified into gas, stellar and black hole phases. DM was modelled as a separate set of particles following N-body physics evolution. The whole simulation consisted of 29 snapshots at redshifts between the initial $z = 20$ and final $z = 0$.

The EAGLE team provides catalogues of dark matter haloes and galaxies identified in the simulation. The dark matter haloes are initially identified from the dark matter particle distribution using a friends-of-friends (Davis et al. 1985) algorithm. Galaxies are then identified from the baryon particle distribution within individual haloes (Springel et al. 2001; Dolag et al. 2009).

In our analysis we used the 100 cMpc³ box. This box size is the best in order to characterise the large-scale environment. We used the snapshot corresponding to redshift $z = 0$ as it is the closest approximation of the observed data, which is in the redshift range $z = 0.02 - 0.05$. The next snapshot in EAGLE would correspond to a redshift of $z = 0.1$.

Similar to the observed data, the r -band absolute magnitude of galaxies

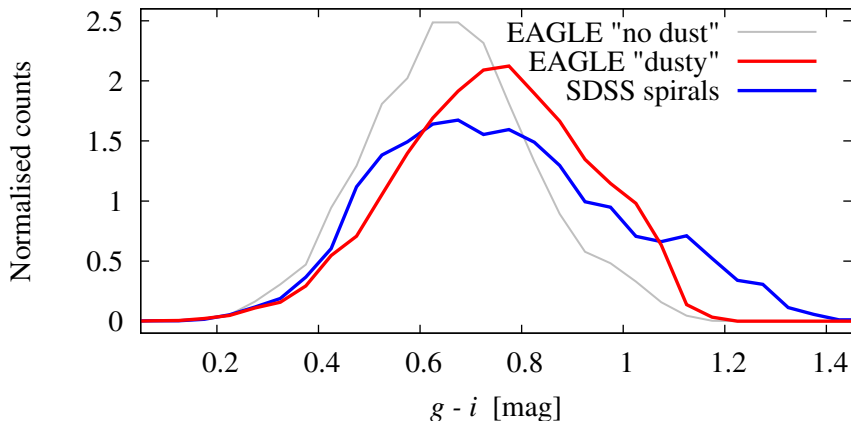


Figure 3.1: Distributions of $g - i$ colours of SDSS spiral galaxies (blue) and EAGLE galaxies that have a dust component in the Camps et al. (2018) catalogue. The colours of EAGLE galaxies are shown without dust attenuation (grey) and with dust absorption when measured from a randomly assigned direction from the galaxy (red).

was used for galaxy selection and for determining brightest group galaxies and calculation of the luminosity density field. For the galaxies, magnitudes with dust attenuation (described in Camps et al. 2018) were used. For galaxies without dust attenuation, the dust-free magnitudes were selected. Dusty magnitudes were compared against SDSS galaxies in different combinations of colours (Figure 3.1). With dust attenuation the match is not exactly the same as can be seen at the blue and red ends of the distribution. EAGLE underestimates the range of colours of spirals compared to SDSS. However, compared to the purely dust-free distributions the difference between the observed and simulated samples are smaller.

For group mass, we used the total mass of all simulation particles within the radius where density is 200 times the critical density of the universe. Stellar mass is the summed mass of all stellar particles within a galaxy. For the gas phase analysis, the coordinates, masses, temperatures, and densities of individual simulation particles were utilised.

3.3 Bisous filament finder

For filament extraction from galaxy catalogues, we used the Bisous method (Tempel et al. 2014b, 2016). Bisous is a marked point process designed to model multi-dimensional patterns. The finder is based on the hypothesis that the filamentary network is modelled by a configuration of connected cylinders. The points are the centres of cylinders and the marks are cylinder shapes and

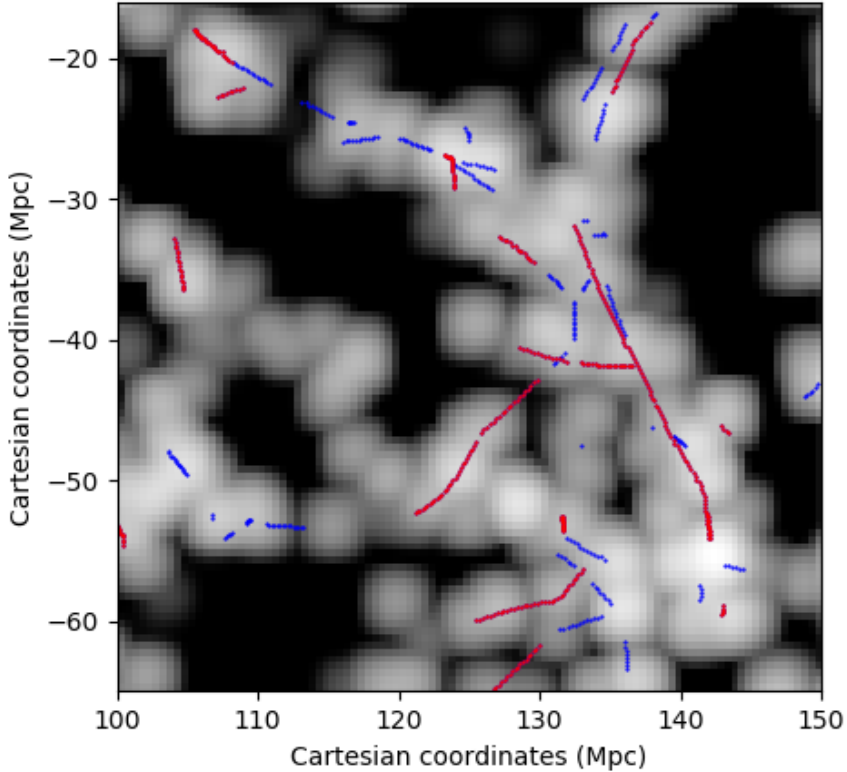


Figure 3.2: 50x50x10 Mpc cut-out from volume-limited SDSS DR12 data. The colour surface plot shows the summed LDF value in the 10 Mpc perpendicular direction. Blue and red lines denote filament spine locations of lengths less than 5 Mpc and equal or more than 5 Mpc respectively.

orientations. Locations of galaxies determine the probability of filaments. The basic methodology is as follows: Filamentary structures are probed with cylindrical shape segments, which are fitted to and adjusted on the galaxy distribution such that the galaxies inside the cylinder radius outnumber the galaxies within two cylinder radii. Nearby cylinders that are well aligned have an attraction parameter connecting individual segments into longer chains. Sharp bends in connected segments are avoided by a repulsion parameter between misaligned cylinders. The process is stochastic, so variations between different Markov-chain Monte Carlo runs of the fitting creates a likelihood map of the most probable filament locations (called the visit map). By default, 1000 runs are made in one instance. Spine locations are defined based on the loca-

tions of density ridges in the visit map. The calculated spine locations we use in this study represent the most likely locations of filament spines. A visual representation of the spines is presented in Figure 3.2. The spine locations are shown as lines in a slice cut-out from the SDSS. The LDF is shown as a colour map.

The filament network is calculated based on the positions of galaxies. In redshift surveys, the redshifts of galaxies in groups and clusters are elongated along the line of sight – the finger-of-god effect. Due to the velocity-based nature of redshift determination, galaxies in virialised structures have different redshifts based on the direction of their motion around the group/cluster potential. Galaxies moving towards the observer have lower redshifts than the group average, while those moving away have higher redshifts. The finger-of-god effect was already suppressed in the galaxy catalogues of Tempel et al. (2014c) and Tempel et al. (2017). In those catalogues, the average redshifts of groups were calculated. In our analysis, we used the group distance as the distance measurement for galaxies within the same groups.

In the Bisous code, the perpendicular distance of a galaxy from the nearest filament spine (D_{fil}) is calculated; an example is shown in Figure 3.3. Galaxies to which the closest filament point is an endpoint of any filament are ignored. These galaxies are typically located either in knots or voids far from any filamentary structures and might bias the results.

Because of the way the Bisous algorithm places cylinders on the distribution of galaxies, filaments tend to be placed in regions where the number of galaxies within a cylinder is larger than the number of galaxies within one and two radii of the cylinders. As a result, the number of galaxies as a function of filament distance has a minimum around one to two cylinder radius values. If the filament distance axis is plotted on a base 10 logarithmic scale, the minimum is enhanced further. This effect can be seen in the bottom panel of Figure 3.3. In our galaxy analysis we chose to avoid this region of the spine distance metric due to larger noise. Galaxies further outside filaments were analysed using the same methods as galaxies inside filament radii, the idea being that the galaxies outside filaments form a control group when measuring filament-based effects.

The performance of Bisous has been tested against other LSS-finding algorithms. Libeskind et al. (2018) compared 12 LSS finders that were available at the time on a uniform set of simulated data. For filaments specifically, they noted that density-distribution widths were in broad agreement but the distribution medians spanned one order of magnitude. They noted larger dispersions in the volume-filling and mass fractions along different methods, with Bisous results being consistently close to the average of the different methods. Rost et al. (2019) compared Bisous filaments with two other methods in the SDSS. They noted that galaxies in filaments have characteristic differences based on the filament-finder method employed. These studies show that there is not yet

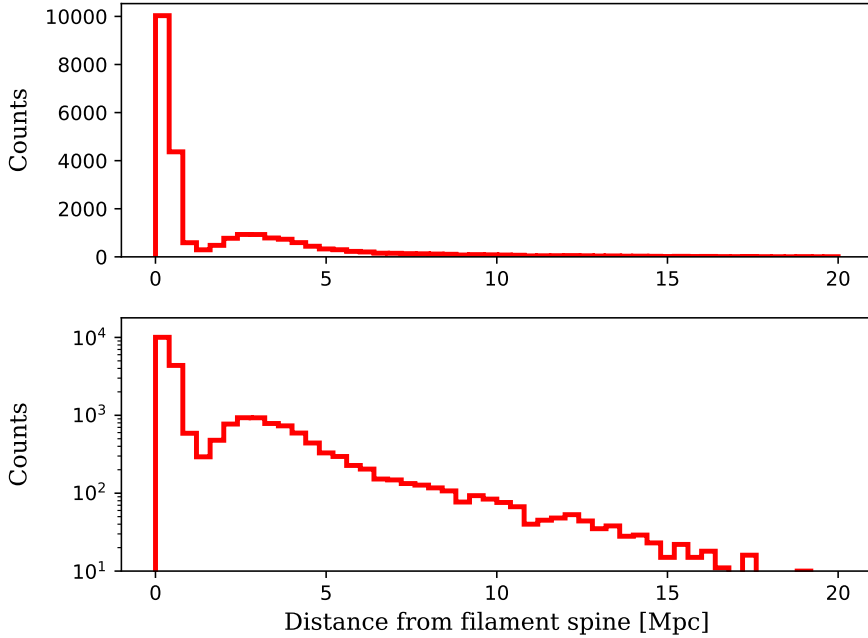


Figure 3.3: Number of galaxies as a function of filament distance in DR12. Both panels show the same data with the y-axis as a linear scale in the top graph and as a logarithmic scale in the bottom graph. The minimum in the number of galaxies between one and two filament radii is visible. In the bottom panel the logarithmic scale visually enhances the difference because of the small number of galaxies at the minimum location.

a uniform method of defining the LSS filaments. We expect future work on the available algorithms to move towards a consensus on defining the various LSS structures.

3.4 Luminosity density field

In observations, the total mass of individual galaxies and galaxy groups is difficult to determine. Most of the mass is contributed by dark matter and, thus, is not directly observable. This mass component can be indirectly measured using the kinematics of galaxies. The kinetic energy of a virialised system can be equated to its potential energy. From this equivalence, the mass of a system can be derived from the radius and velocity dispersion of its constituents (Tempel et al. 2014c). Group sizes and velocity dispersions are typically measured quantities in galaxy redshift surveys, including the catalogues described above. However, the accuracy of dynamically determined masses depends on the number of group members. Thus, dynamical mass estimates are less accu-

rate for poor groups consisting of only a few galaxies.

Another method often used to determine group masses is Halo Abundance Matching (HAM). This method is based on the assumption that halo masses and galaxy properties are correlated. The basic idea is that the most massive galaxies are located in the most massive haloes. This method has been calibrated in simulations and has been shown to be able to reproduce spatial clustering properties of galaxies (e.g. Kravtsov et al. 2004; Conroy et al. 2006; Behroozi et al. 2010).

In our research, the definition of the environment, that is the halo mass, is inferred from the luminosity density field (LDF), which is calculated from the optical luminosities of the galaxies. The LDF acts as a tracer of matter density in each volume element by smoothing the distribution of light emitted by galaxies over a spherical kernel. The LDF value can be calculated at any point of interest within the volume, e.g. at the galaxy locations themselves. With this method, smaller structures are essentially spread out to provide a measurable quantity for larger structures. A visual representation of the LDF within the SDSS can be seen in the slice cut-out in Figure 3.2. The LDF is shown here with a colour map with white areas corresponding to regions of higher LDF value.

The LDF approach is similar to the HAM method described above; however, it is more robust and does not need to be calibrated with simulations since a relative density scale is sufficient for comparing galaxies in the same catalogue.

To determine the luminosity density field (LDF), the method outlined in Liivamägi et al. (2012) was followed. The light (in units of 10^{10} Solar luminosity) of each galaxy is spread out over a spherical area with a B3 spline kernel profile. This kernel is similar to a Gaussian, except instead of terminating at infinity, it has discrete defined ends. The mathematical methodology is described in detail in Liivamägi et al. (2012).

The radius of the kernel determines which structures are traced by the LDF. Previously, this method has been used in defining and studying the supercluster–void network (e.g. Liivamägi et al. 2012; Lietzen et al. 2012) with $8 h^{-1}\text{Mpc}$ scaling. Smoothing over this large scale loses detail on the smaller structures of interest in this study – the groups and filament cross-sections. Nevalainen et al. (2015) used the LDF with $1 h^{-1}\text{Mpc}$ scaling in order to look for missing baryons in cosmic filaments.

The radius of the smoothing kernel here is chosen to coincide with typical group radii, 1.5 Mpc or roughly $1 h^{-1}\text{Mpc}$ (Einasto et al. 2018). Thus the LDF-based local environment is defined by its constituent galaxies both in terms of luminosity contribution and spatial distribution. Fainter group members and galaxies further separated from the centres of groups contribute less to the group LDF. Thus, the bright centrally located galaxies, which are usually more massive, contribute most to the local environment.

We normalise the luminosities to the median luminosity density of the volume of the galaxy sample. Thus, while absolute group masses are not determined, the LDF of different catalogues can be compared when assuming a similar luminosity distribution of galaxies. The use of this method in group mass estimation is described in more detail Paper II (Section 3.2 and Figure 1 in that paper). For studying the gas phase in the EAGLE simulation in Paper III, a larger radius for the LDF kernel of 2 Mpc is used in order to probe the regions outside of galaxy groups for the WHIM.

3.5 Galaxy and filament selection

The Bisous filament finder is designed to look for configurations of galaxies based on their position. As it is a stochastic process by nature it can misidentify certain galaxy configurations as filaments. This is additionally complicated by the amount of free parameters in its input file that are not fixed and need to be fine-tuned to the problem under study (Tempel et al. 2016). For this work, the input was set up with values that were previously tested to result in filament spines that correspond well with observed galaxy positions in the SDSS data.

Due to the large number of galaxies in the datasets, the derived filament catalogue contained a significant amount of spurious spines. These typically short spine segments would be located both in sparsely populated voids and dense clusters. The catalogue needed to be refined to select a sub-sample of robust filaments. Below, some specific considerations in filament and galaxy selection in each published paper are summarised.

In the future, when the Bisous algorithm and its behaviour is studied in greater detail, some of the misidentified spines could already be avoided when configuring the finder to certain datasets. A detailed analysis of the behaviour of Bisous and the effects of input parameters has not been a goal of this work and is left to other researchers and future work (e.g. Muru & Tempel 2021).

3.5.1 Specifics in Paper I

The SDSS DR10 galaxy catalogue and the Bisous filament catalogue used in Paper I are available in CosmoDB (<http://cosmodb.to.ee>), the Tartu Observatory cosmology-related catalogue database. The related publications for the catalogues are Tempel et al. (2014a) for the galaxy catalogue and Tempel et al. (2014b) for the filament catalogue. Below, the information relevant to Paper I is summarised.

In Paper I, galaxies from the SDSS DR10 in two luminosity bins were considered: a brighter ($M_r < -20$ mag) and a fainter ($-18 \text{ mag} > M_r > -20$ mag) sample. The samples cover distance ranges up to $h^{-1}\text{Mpc} < 320$ and $h^{-1}\text{Mpc} < 135$, respectively. Both samples have a near cut-off at $60 h^{-1}\text{Mpc}$ (corresponding to redshift $z \approx 0.02$). The LDF at galaxy locations was used

with the contribution of the galaxy itself removed from the field value. This was done in order to define the local environment of galaxies independently of the galaxies' own properties.

The filament finder was run on the full flux-limited galaxy catalogue. The drawback of flux-limited data is the decrease in galaxy number density with distance. Indeed, a group-distance-related effect was noted as a function of filament distance (Figure 1 in Paper I). This was accounted for along with the local environment as described below.

In order to measure the proximity of galaxies to filaments, we used the D_{fil} of each galaxy. Galaxies were divided into bins of D_{fil} . The bins were chosen to contain roughly the same number of galaxies. In total, six bins inside and six outside the filament radii were used, with roughly 5000 galaxies per bin in the brighter sample and 900 in the fainter. To normalise the environment of galaxies, we firstly excluded about 5% of galaxies which were in environments with extreme densities (high or low). For the remaining galaxies, the LDF and group distance distributions in each bin were normalised to the full sample distribution by applying a weight to each galaxy so that galaxies in less-typical environments and at less-typical distances gained a smaller weight. The averages of weighted distributions are shown in figures in Paper I and in Chapter 4. Not all parameters were distributed normally in the bins, but averages were chosen as a good first estimate of the entire dataset.

Filaments were probed using cylinders of $1 h^{-1}\text{Mpc}$ diameter. To sample only strong filaments, only filament spine lengths of $15 h^{-1}\text{Mpc}$ and longer were considered. Bisous finds filaments with a pre-set radial range. Besides the $1 h^{-1}\text{Mpc}$ diameter catalogue, Bisous filaments with $2 h^{-1}\text{Mpc}$ and $4 h^{-1}\text{Mpc}$ diameters were used in the analysis. With filaments of larger diameters than $1 h^{-1}\text{Mpc}$, the results were quantitatively similar to those presented below, but showed weaker trends. We omitted the results derived from thicker filaments and focused on those of $1 h^{-1}\text{Mpc}$ diameter, as these filaments are of most interest in terms of galaxies in groups.

3.5.2 Specifics in Paper II

In paper II, a new catalogue based on SDSS DR12 was used as the base galaxy catalogue. In this catalogue, galaxy group determination was done with a more refined algorithm, as described in Tempel et al. (2017). The area and main galaxy content is the same as in the DR10 catalogue. It is also available in CosmoDB.

Only one volume-limited sample was selected for analysis, containing galaxies with absolute luminosities of $M_r < -19$ mag in the r -band. Compared to Paper I, this selection offered a compromise between the volume of the brighter sample and a broad range of luminosities of galaxies probed. The sample covers a distance range between 85 Mpc and 215 Mpc. Galax-

ies without stellar mass and SSFR estimates were excluded, along with those that had unrealistic colours in $g - i$ and $u - z$ bands. As a result of these selections, a small number of galaxies were excluded. In the Tempel et al. (2017) catalogue, galaxy parameters are presented assuming the Hubble constant $H_0 = 67.8 \text{ km s}^{-1} \text{ Mpc}^{-1}$, and the data in Paper II follows that scaling.

The LDF was calculated with only the volume-limited sample galaxies contributing in order to avoid distance-based effects. The 1.5 Mpc smoothing radius was chosen, which is close to the $1 h^{-1} \text{ Mpc}$ smoothing used for Paper I. The LDF value at BGG locations was determined to be a good tracer for halo masses for the filament groups (Section 3.2 in Paper II). This estimate was used to characterise the local environment as most groups had too few members for reliable dynamical mass estimation.

For isolated galaxies, the luminosity density versus halo mass relation is not as reliable. In the EAGLE simulation, at halo mass below $12.5 \times 10^{10} M_\odot$, the dispersion of the relation between halo mass and LDF value becomes wide. There were too few isolated galaxies with higher mass for a statistical analysis. Thus, halo masses of isolated galaxies could not be reliably constrained with this method. A similar study of satellite galaxies has been left for future work when more data becomes available.

The performance of the Bisous algorithm is based on the number density of galaxies (Muru & Tempel 2021). In order to avoid the distance-based effects that were noted in Paper I, the algorithm was run on the selected volume-limited galaxy sample. Development in the Bisous code allowed for more flexibility in selecting the filament radius. The range of radii of the cylinders used to construct the filament network was set with a minimum-to-maximum range of 0.5–1.0 Mpc.

For filament selection it was important to include a sufficient number of filaments (and by extension total number of galaxies within filament radii) while excluding unreliable and spurious spines from the analysis. We required filament spine lengths to be above 5 Mpc to ignore spurious spines that the Bisous code finds inside voids and clusters. An example of spines of different lengths can be seen in Figure 3.2. Selection by spine length narrowed the range of environmental densities (defined by the average of the 1.5 Mpc smoothed LDF along filament spines) within the filaments (see Figure 2 in Paper II). Longer spines are situated in a narrower range of environment densities. Some of the selected filament spines were visually checked and compared with galaxy distributions. The filaments retained were seen to correspond well to visually distinguishable filaments of galaxies.

The range of LDF values decreases rapidly at a distance of 4 Mpc from filament spines, indicating locations inside deep voids. As a result, we could not compare the local environments of galaxies nearer and farther than 4 Mpc and excluded the farther galaxies from analysis.

Galaxies in each group were ranked based on r -band luminosity. The

brightest galaxy in each group was tagged as the BGG for analysis. In the final analysis there were 1382 BGGs in 976 filaments.

3.5.3 Specifics in Paper III

In Paper III, EAGLE simulation data was used to study the intergalactic medium in filaments, specifically the hot WHIM at temperatures above $\log T(K) > 5.5$. We used the 100 cMpc³ simulation as a base. In our analysis, the galaxy catalogue described in McAlpine et al. (2016) and particle data described in The EAGLE team (2017) were used.

The galaxy sample was selected to match the observed sample in Paper II. EAGLE has a slightly lower number density of galaxies compared to the SDSS at the same luminosity cut. In order to ensure the filament sample would be in accordance with the observed data, EAGLE galaxies were selected with a luminosity limit of $M_r < -18.4$ mag, matching the number densities of the two samples.

We utilised the galaxy LDF as an observational trace for potential sites of the hot WHIM. In order to better probe the intergalactic medium outside of groups, a smoothing scale of 2 Mpc was chosen for the LDF.

Filaments were detected using the Bisous algorithm based on galaxy positions in the luminosity-limited catalogue. Spines shorter than 2 Mpc were excluded from further analysis, as most of these are in high-density regions, likely in clusters instead of filaments. In total 743 spines were considered in the analysis.

3.6 Statistical comparison of SDSS and EAGLE galaxies

Some of the results presented in this thesis are based on real (SDSS) data, and some on simulated (EAGLE) data. To make sure that the corresponding filaments are comparable, we made several statistical tests comparing the SDSS and EAGLE galaxy samples.

When comparing observations and simulations, one has to consider important shortcomings in both data samples. As discussed in Chapter 1, observations suffer from unobserved galaxies and measurement errors, while simulations contend with finite resolution and detail in the attached galaxy evolution physics. This results in both observations and simulations needing a reasonable cut-off for galaxy selection.

Some methodologies we applied to get comparable samples of simulated and observed galaxies are presented below. The resulting data are presented as comparisons of different property distributions of galaxies and filaments in both datasets.

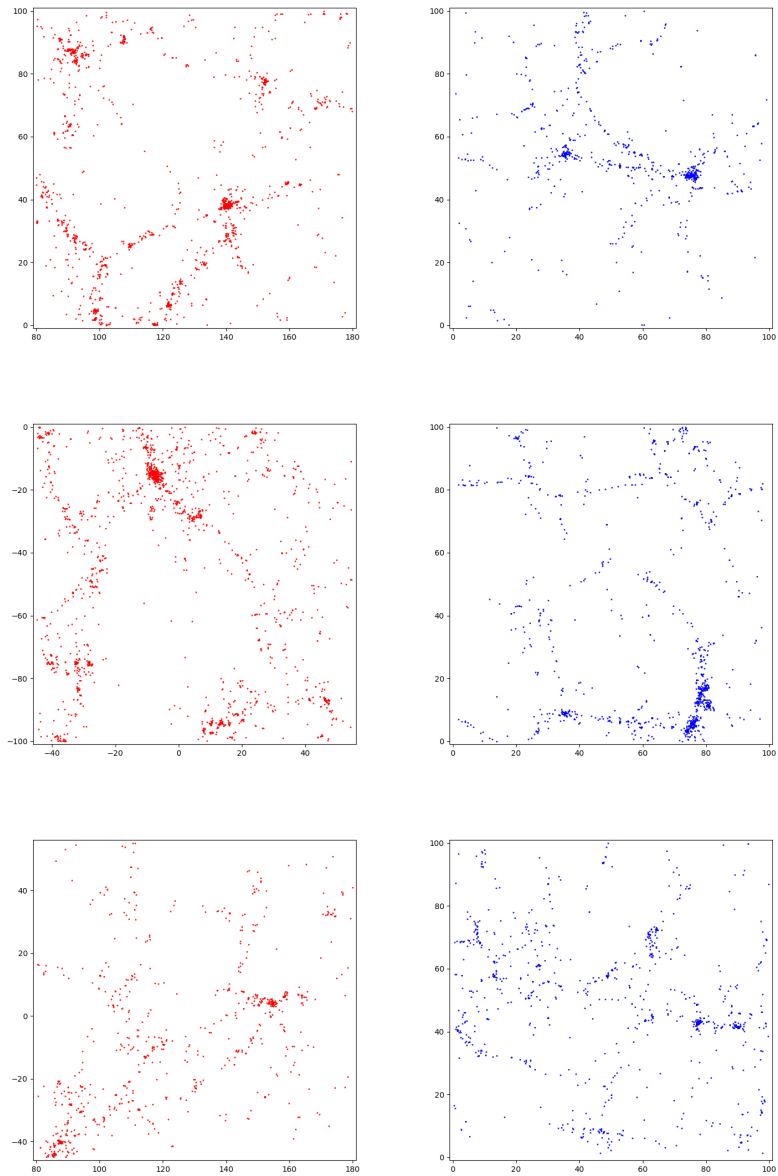


Figure 3.4: A selection of real-space slices with 100 x 100 Mpc side length and 10 Mpc thickness showing distributions of SDSS (red) and EAGLE (blue) galaxies. The samples have matching number densities. The slices shown in this figure were hand-picked to show regions with visually similar galaxy distributions in both samples.

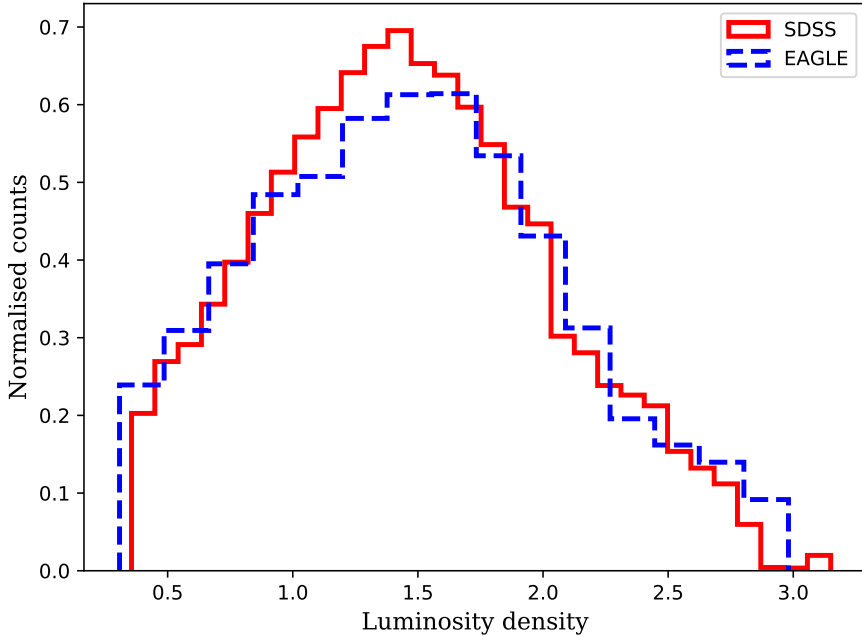


Figure 3.5: Real vs simulated galaxy distributions of the LDF values at galaxy locations for the SDSS and the EAGLE samples. The EAGLE sample matches well with the SDSS.

3.6.1 Galaxy number density

In observations, the luminosity limit of observed galaxies effectively means that at each distance, only galaxies above a certain absolute luminosity are observed. In order to have a sample that has a complete range of luminosities, further, brighter and nearby, fainter galaxies have to be excluded. A volume-limited selection of SDSS galaxies thus needs luminosity-based and distance-based cuts. In the comparison below, the starting point was to define the limiting luminosity as -19 mag in the r -band. The motivation for this limit is the compromise it offers in terms of the total volume covered and the broad range of galaxy luminosities usable in other analysis; it corresponds to the volume-limited sample used in Paper II. In the SDSS, this luminosity cut corresponds to a distance cut of 215 Mpc or redshift $z = 0.05$.

The peak observed magnitude of nearby galaxies saturates the SDSS cameras. Nearby, bright galaxies were excluded from SDSS catalogues or flagged as unreliably measured and not considered in our analysis. Because of this limitation, there is an effective lower limit distance of a volume-complete galaxy catalogue at around 85 Mpc, corresponding to a redshift of $z = 0.02$. There are other considerations for why the nearby volume is not useful for LSS stud-

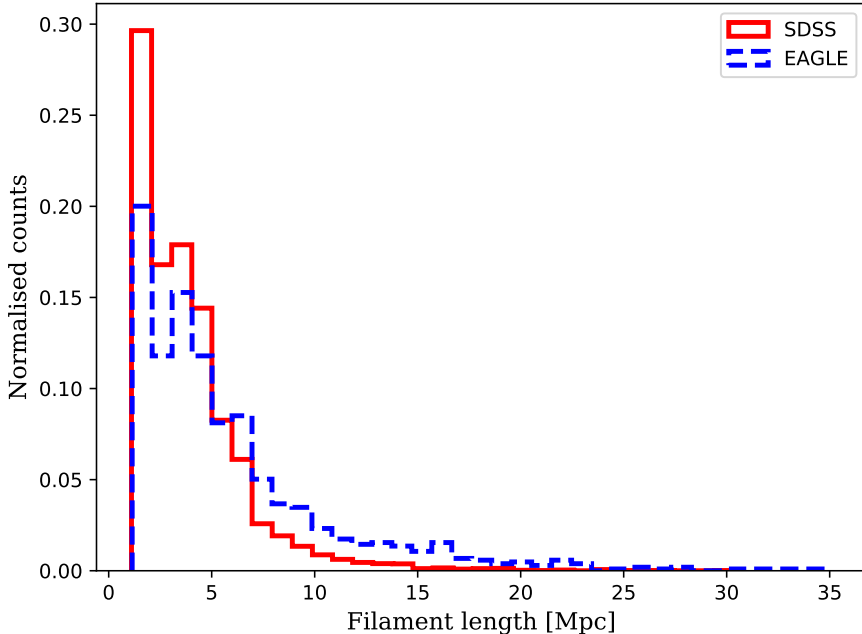


Figure 3.6: Real vs simulated distributions of filament lengths. The EAGLE sample contains a slightly higher number of longer filaments.

ies. Firstly, in the nearby volumes, filament finders are unreliable due to the small volume considered. Secondly, Hubble expansion is slower in the nearby cosmic volume, meaning redshift measurements are less reliable proxies of distance. The luminosity-based lower limiting distance is also a good cut-off for our filament sample. The final volume-limited SDSS catalogue contains 55973 galaxies in a volume roughly $6.8 \times 10^6 \text{ Mpc}^3$, and a galaxy number density of 0.0082 Mpc^{-3} .

Using exactly the same luminosity limit as in SDSS, at -19 mag in the r -band, results in comparatively lower number densities in EAGLE (0.0062 Mpc^{-3}). The galaxy number density is the primary parameter in determining the performance of the Bisous filament finder (Muru & Tempel 2021). In order to obtain filaments with similar properties to observed ones, it was important to adjust the EAGLE galaxy sample correspondingly. Our workaround with EAGLE data was to use a slightly fainter luminosity cut than in SDSS – -18.4 mag in the r -band – and this yielded a match in the number densities. This selection contains 8633 galaxies in the 100^3 Mpc^3 volume, resulting in a number density of 0.0086 Mpc^{-3} .

Visual inspection shows a good match between the two samples (Figure 3.4). EAGLE reproduces groups and smaller clusters of similar shape and dimensions as those that are observed. Larger clusters and superclusters, like

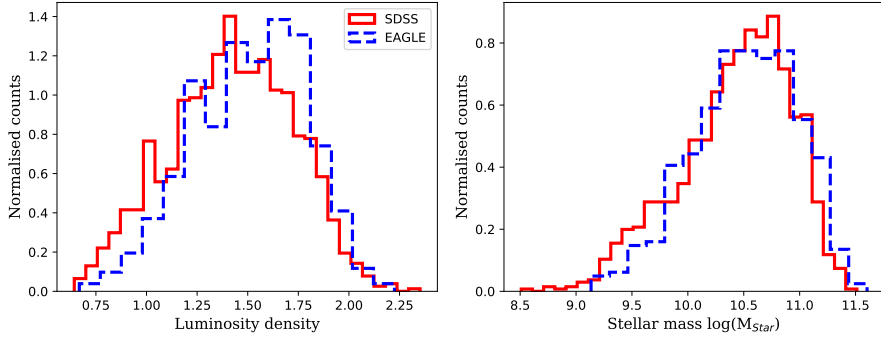


Figure 3.7: Real vs simulated galaxy distributions of the LDF values at the locations of brightest group galaxies in our filament sample (left), and stellar masses of the same galaxies (right). Some differences in the data can be noted, with EAGLE having slightly higher average LDF values. Also, at the lower end of both distributions, EAGLE has systematically lower values.

those observed in sky surveys, are not reproduced in EAGLE. The simulation box is too small to create some of the larger structures known to form in the cosmic web. Filaments are also visible in the galaxy distributions of both samples. Filament lengths and distributions appear similar in the samples; however, EAGLE filaments appear slightly narrower compared to those of the SDSS.

The 1.5 Mpc smoothed LDF distributions at galaxy locations match well in this scenario, as can be seen in Figure 3.5. The distributions are similar with only slight differences. Figure 3.6 shows the distributions of filament lengths calculated based on the two datasets. EAGLE contains a relatively higher fraction of long filaments and lower fraction of short filaments compared to the SDSS. However, the total number of filaments (7864 in SDSS and 1092 in EAGLE) are roughly equal when accounting for the difference in volume of the two samples.

In this thesis, the brightest group galaxies have been of particular interest. In Paper II, EAGLE was used as a test for the applicability of the LDF field as a trace of the local environment. As a basis for comparison, we looked at the observed and simulated LDF and stellar mass distributions of these galaxies (shown in Figure 3.7). The samples are generally in agreement, with only minor differences in averages and the wings of the distributions. The data shows that EAGLE BGGs are similar enough to observed galaxies for direct comparison of these samples.

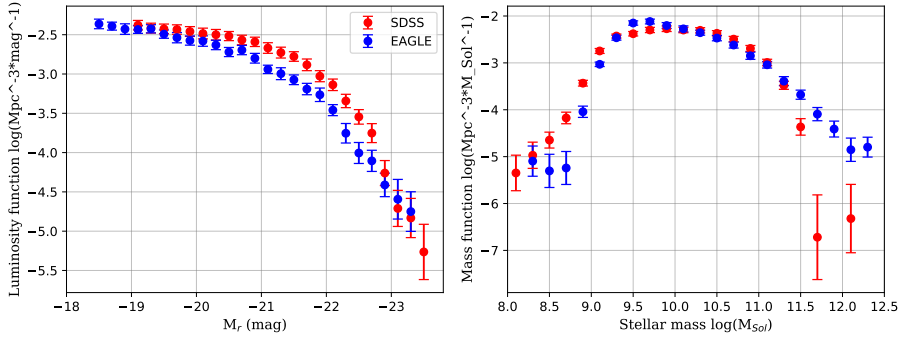


Figure 3.8: Real vs simulated galaxies luminosity (left) and mass (right) functions. Errors show the variance within the respective data from 100 randomly placed sub-spheres, with 50 Mpc radius, within the full volume. The EAGLE sample has consistently lower number of galaxies at most luminosities. The number of the most massive galaxies is higher in EAGLE.

3.6.2 Luminosity and mass functions

The luminosity function (LF) is the measure of the number density of galaxies as a function of their luminosity. The LF has been used as an important tool in understanding galaxy evolution (Yang et al. 2003; Cooray & Milosavljević 2005; Hansen et al. 2009). The mass function is the analogue of the LF in stellar mass. These functions give a general overview of the types of galaxies in a volume. Luminosities and masses are often measured and provided in galaxy catalogues, thus making them handy first-look tracers when comparing different datasets.

Instead of global functions, which consider all galaxies in the dataset, we used randomly selected subregions of the full volume in order to account for cosmic variance. This enables us to account for local variability of the data and the variance is presented in the figures below as 1σ errors on top of the calculated functions. Sub-volumes were designated as spherical in shape, because spheres are straightforward to randomly place into the conical shaped contiguous Sloan volume without crossing the survey edges.

The luminosity and mass functions are shown in Figure 3.8. At matching number densities, the luminosity function of EAGLE galaxies stays lower compared to SDSS. In the right panel, the EAGLE stellar mass function shows a more rapid drop at the low mass end compared to SDSS.

The discrepancy in number densities discussed in the previous section is visible at the high end of the luminosity functions of SDSS and EAGLE in Figure 3.8. Compared to observations, luminosities of EAGLE galaxies are underestimated. Trayford et al. (2015) noted the same discrepancy for the $z = 0.1$ snapshot in EAGLE. Differences in mass functions are noted in Schaye et al.

(2015), but they also remark that this is acceptable, as the overall agreement between simulation and observations is within 0.3 dex, which is in the uncertainty range of stellar evolution models of the simulation. Even with these differences in observations and simulations, EAGLE represents a large improvement over previous simulations in generating stellar populations of galaxies comparable to observations solely from initial conditions.

CHAPTER 4

RESULTS

Here we present the results from the published papers. At the beginning, our focus was on a broad sample of galaxies and the filament effects that could be deduced from that sample. In the second part, we concentrated on the sub-population of brightest group galaxies, which are important and tend to dominate the galaxy group environment. Finally the Bisous filament-finder method is expanded upon; using simulation data, its usefulness as a filament finder is reinforced. The baryons in filaments outside galaxies are also examined, which is the other side of the filament–baryon connection in this thesis.

The figures from the thesis papers are not reproduced here; instead we refer to the relevant figures in the papers when discussing them. Errors in the figures are derived using 1000 bootstrap resamples with replacement unless otherwise specified.

4.1 Properties of galaxies in filaments.

We gauge the potential effects that filaments have on galaxies by measuring averages of galaxy properties in bins of distance from the filament spine (D_{fil}). The brighter $M_r < -20 \text{ mag}$ and fainter $-18 > M_r > -20 \text{ mag}$ samples are presented with red circles and green squares respectively in Paper I and the figures discussed in this section. Each galaxy’s contribution to property averages is weighted accordingly, as discussed in Chapter 3.5.1. In the figures, bars and lines show bootstrap deviation from the average, with 1σ and 2σ confidence respectively. Vertical, dashed lines in the figures of Paper I and in this section mark the separation of samples inside and outside the fixed filament radius of $0.5 h^{-1}\text{Mpc}$.

For all galaxies, weighting of samples based on LDF values and group distances removes large variations in the different D_{fil} bins of these parameters (shown in Figure 1 in Paper I). The same weights were applied when calculating the averages of the other properties presented below. With local environments and distance-based variations in the data accounted for, any residual trends in the weighted data should originate from the filament environment.

There is a noticeable change in the relative fractions of elliptical and spiral morphologies of galaxies in filaments (Figure 2 in Paper I). For galaxies brighter than $M_r < -20 \text{ mag}$, the ratio of elliptical to spiral morphologies increases closer to filament spines. Near the spine, the fractions are almost equal, while for galaxies outside the filaments, the elliptical fraction drops below 35 percent. Outside the filament radius the ratio is almost independent of filament distance. In agreement with the morphological change, a reddening

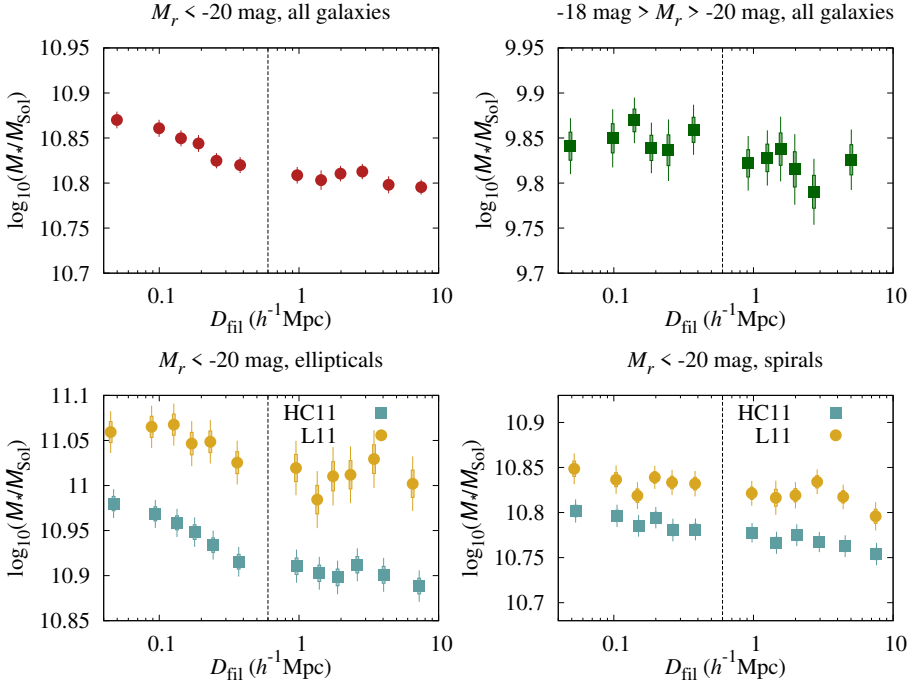


Figure 4.1: Average stellar mass in bins of filament distance. The panels show brighter, fainter, elliptical and spiral (in the brighter sample only) morphologies. Bars show 1σ and lines 2σ variance of the data based on 1000 bootstrap resamples with replacement.

trend toward spines exists for galaxies in $g - i$ colours (the left panel in Figure 3 of Paper I).

The fainter samples of all parameters show little to no trends within the bootstrap error ranges. This indicates that either the variance in the data is too broad to effectively detect the trends, or alternatively, galaxies in the fainter sample do not experience the filament-based trends discussed above.

In order to determine if besides the morphological transformation other galaxy properties are modified inside filaments, we plot the binned averages of elliptical and spiral galaxies separately in the brighter sample. We utilised both available morphological classifications. We used the L11 definition of spirals and ellipticals and omitted galaxies with undefined morphologies. In the case of the HC11 definition, we determined the morphology of a galaxy if its fractional morphological classification was more than 50% likely to be either of spiral or elliptical morphology. When looking at elliptical and spiral galaxies separately, the $g - i$ colour trend remains for both populations, with spirals showing a stronger reddening trend compared to elliptical galaxies.

Galaxy properties are often dependent on the stellar mass of galaxies.

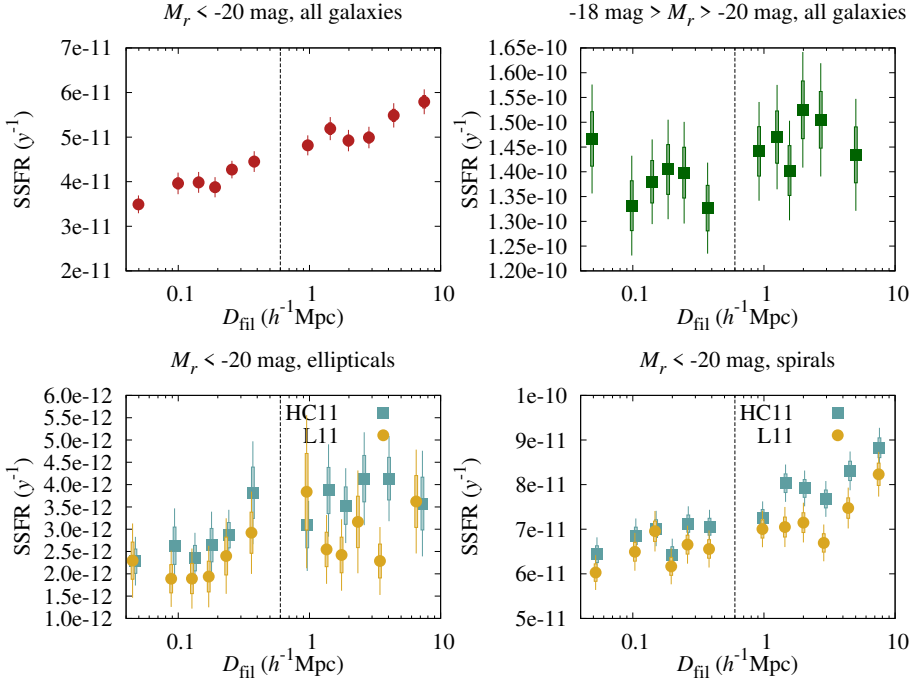


Figure 4.2: SSFR averages split into four panels as in Figure 4.1.

We show the weighted stellar mass trends of our sample in Figure 4.1. A minor residual stellar mass trend is visible inside the filament radius in the brighter sample. However, this trend represents a minor change in absolute masses. We tried additionally weighting our sample by the stellar mass, but the other trends did not change noticeably. Morphological separation shows that the mass increase comes mainly from elliptical galaxies, as seen in the lower left panel in Figure 4.1.

Corresponding to morphology and colour, the SSFR of galaxies decreases towards filament spines, as shown in Figure 4.2. This trend seems mainly driven by the change in properties of spiral galaxies, as seen in the lower right panel of this figure. Spiral dominance in this property is expected as elliptical galaxies tend to be more massive and passive with minor star-formation activity.

Interestingly, the D4000 index seems to change more outside of filaments, while inside filaments, the trends are almost reversed (Figure 4.3). The time since the last episode of star formation increases towards the spine until the innermost bins close to the filament spine are reached, at which point the D4000 value decreases. This change seems to be driven mostly by spiral galaxies; however, ellipticals, as determined by HC11, that are outside filaments also show a similar trend. However, there is no similar transformation for other

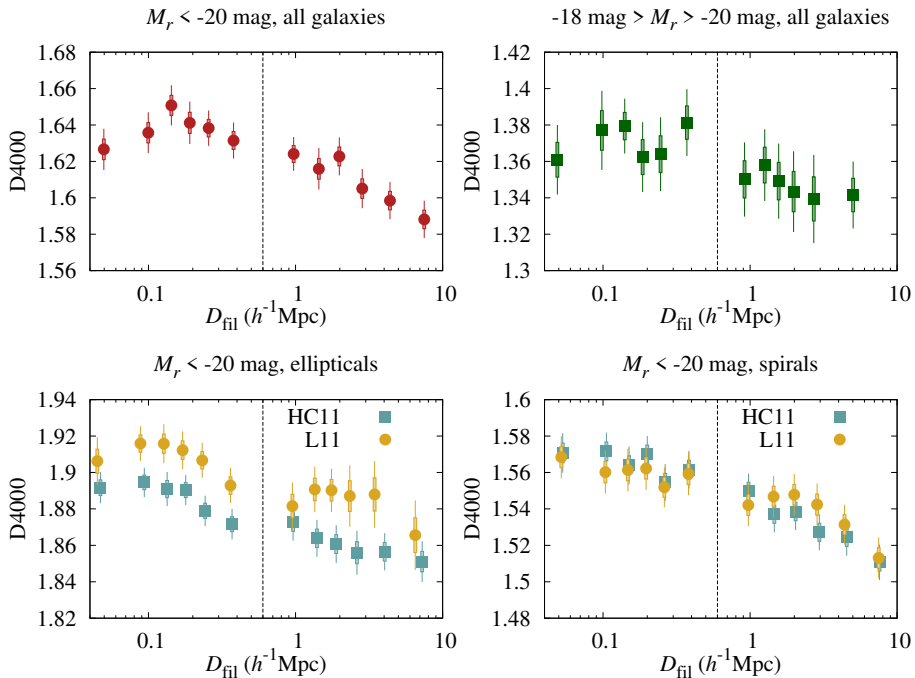


Figure 4.3: 4000Å break averages split into four panels as in Figure 4.1. The y-scale is linear and has the same absolute range in each panel in order to better compare the datasets by eye.

galaxy properties. The variation within the filament is within 2σ errors, so random variation in the data cannot be excluded as a cause.

The concentration index of all galaxies increases towards spines (Figure 4.4). Morphological separation shows weaker trends in the elliptical and spiral populations. Stellar velocity dispersion also increases (Figure 4.5), which persists for separate morphologies. Elliptical galaxies experience a larger increase in filaments, but spiral galaxies also become dynamically hotter to a lesser extent.

Overall, the trends of most properties show a significant change inside the filament radius. With the exception of the D4000, other properties of galaxies indicate a change consistent with increased environment density. With the environment accounted for by weighting based on the LDF value, these changes in the properties of galaxies indicate separate processes acting on galaxies inside filaments.

For the fainter galaxies, which are found in the brightness range $-18 < M_r < -20 \text{ mag}$, no strong trends appear with respect to filament spine distance. The fainter sample contains fewer galaxies and has correspondingly larger errors. As a result, we could not make conclusions about filament-based

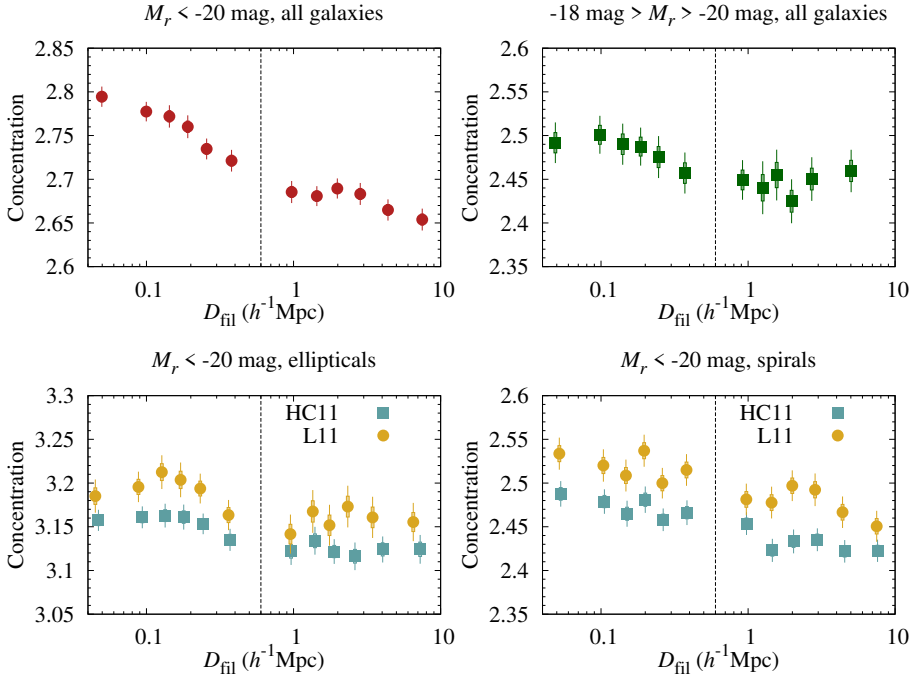


Figure 4.4: Concentration index averages split into four panels as in Figure 4.1. The y-scale is linear and has the same absolute range in each panel in order to better compare the datasets by eye.

effects in this sample. A larger sample derived from a deeper sky survey would be useful in probing galaxies in this brightness range in the future.

4.2 Group properties and brightest group galaxies in filaments.

Motivated by the filament-based trends described in the previous section, we focus on sub-populations of galaxies. BGGs are of particular interest for studying filament-based effects due to their specific (more uniform) nature and location within the local halo. The catalogues and methodology used are described in section 3.5.2.

While selecting for reliable filaments in medium density environments it was revealed that groups in filaments tend to be poor, with about 95% of groups in the selection having fewer than five members within the volume limited catalogue. To be able to also assess poor group environments, we preferred the LDF over dynamical mass estimates. Using the EAGLE simulation as a test sample we show that the LDF value with 1.5 Mpc smoothing at the locations of BGGs shows a linear correlation with total group mass (baryonic plus dark matter). The correlation is described in more detail in Section 3.2 and the

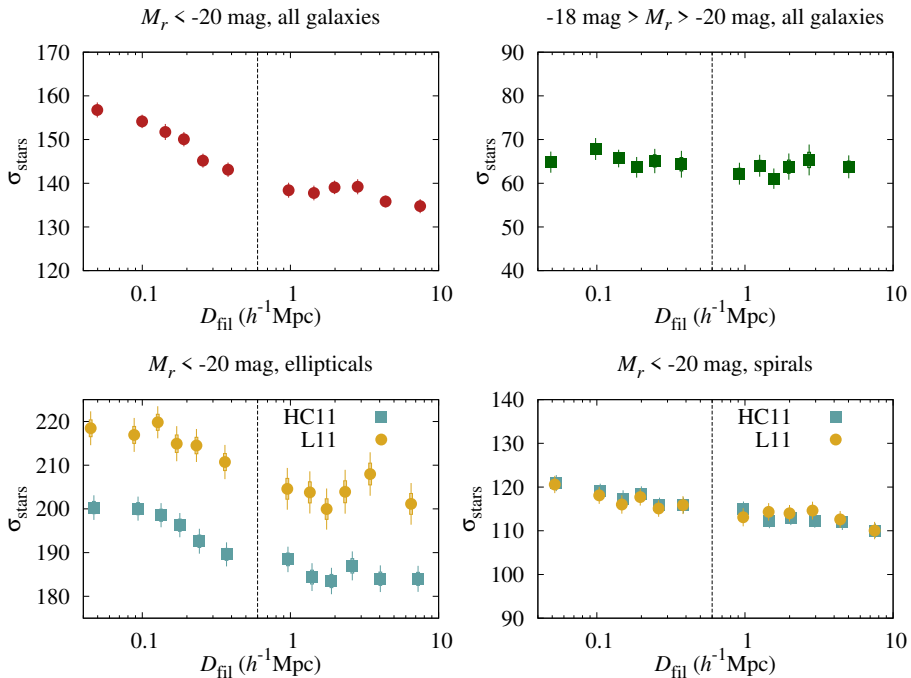


Figure 4.5: Stellar velocity dispersion averages split into four panels as in Figure 4.1. The y-scale is linear and has the same absolute range in each panel in order to better compare the datasets by eye.

related Figure 1 in Paper II.

The impact of the filament environment was compared to that of the local environment (Figure 3 in Paper II). The filament was characterised by the perpendicular distance of BGGs from filament spines, and the environment was measured by the LDF at BGG locations. The BGGs were divided into sub-groups based on some characteristic properties: colour, stellar mass, morphology, and star-formation activity. As expected, the local environment is the main determining factor of galaxy properties. We checked the average distances of the different sub-populations from filaments in bins of constant environment distance (Figure 4 in Paper II). However, none of the galaxy properties showed significant variance in filament distance, and the median properties of BGGs do not show filament-based variation.

We wanted to confirm that there are no variations within the distributions that remain hidden in the medians presented above. For this, the BGGs were split into two bins – one inside the filament radius and another outside. The goal here was to see if the distribution shapes of BGG properties are different inside and outside filaments.

The filament radius was a free variable (ranging between 0.5 and 1 Mpc)

during filament detection. We separated the BGGs based on the filament radius into an inner sample (containing 1158 BGGs) within the filament radius and an outer sample (153 BGGs) between two filament radii up to 4 Mpc from the spine. A gap was left between the inside and outside samples to avoid overlap between populations and also to avoid the minimum in galaxy distribution as a function of spine distance (described in Chapter 3.3).

The resulting distributions were compared in Figures 6, 7, and 8 in Paper II. Figure 6 shows the match between the LDF and stellar mass, which are the main drivers of galaxy properties. The property distributions match well within the error ranges, adding confidence to the idea that the two populations represent BGGs of similar local environment and mass. Likewise, we find that the star-formation indicators (SSFR and D4000) and the colours of BGGs (Figures 7 and 8) do not vary significantly between the two populations. Local differences across the distributions reached only 1σ significance. A two-sample Kolmogorov–Smirnov test was run on each pair of distributions and confirmed no statistically significant variations in BGG properties.

These tests show that BGGs with similar local and stellar mass content experience no significant filament-based effects on their other properties. This result is in contrast to previous findings in Paper I, which showed significant change in all bright galaxies within and outside filaments. We address this contrast in the discussion section below.

4.3 Intergalactic diffuse gas in filaments

The Bisous method was applied to simulated galaxies with the goal of determining observational traces for the hot phase of the WHIM. In filaments, the relatively higher concentration of the dark matter draws the intergalactic gas nearer to them due to gravitational attraction. The gas is shock heated to temperatures above 10^5 K. Thus, the WHIM is expected to reside in filaments. Simulations show that outflows from galaxies enrich the intergalactic medium, making it observable through absorption lines of highly ionised metals. Motivated by this scenario, the existing Bisous toolset was applied to the EAGLE simulation to explore the basic thermodynamic properties of the intergalactic medium and establish observational traces of these diffuse baryons. Applying the filament finder on simulated galaxies gave us an excellent opportunity to test the robustness of the galaxy-based Bisous-detected filaments. EAGLE particle data could be used for confirming the locations of filaments that are also in intergalactic gas distributions. The sample of simulated galaxies was selected for comparison with to SDSS $M_r < -19$ mag as was used in Paper II. The EAGLE limiting magnitude was set at $M_r < -18.4$ mag to match the number densities of galaxies between the two datasets. The motivation for this selection is outlined in Chapter 3.6. We refer to figures in Paper III in this section.

In Figure 7, a visual representation of the match between Bisous-detected filaments and the missing baryons in the simulation are shown. The panels in the figure show the same 5 Mpc thick slice from the simulation volume. Galaxies are shown with blue points and filament locations in grey. The colour map in the lower left panel shows the missing baryons captured with the filament finder. The lower right panel shows the filament spines with high LDF values in blue overlaid on the missing baryons shown with a colour plot. The filament spines coincide with missing baryon concentrations, with high LDF spines tracing the denser gas filaments.

We compared the luminosity overdensity distributions between SDSS and EAGLE. In Figure 10, the average luminosity overdensities of filaments are compared between filaments in the observed and simulated samples. The distributions are similar, with minor differences after accounting for difference in volumes. The EAGLE distribution was divided into three sub-samples based on the luminosity overdensity value, with the high overdensity sub-sample, containing 77 filament spines, of specific interest in the search for observational signals in the WHIM.

The usability of the luminosity overdensity sample as a WHIM trace is shown in Figure 11. The top panels show the absolute and relative distributions of the gas mass as a function of temperature within Bisous filaments. The distributions are divided based on the luminosity overdensity. The high overdensity sample traces a larger fraction of the high-temperature phase where the missing baryons reside. The high-luminosity range of the LDF is thus an useful observational trace of the missing baryons.

Figures 13 and 15 show profiles of gas temperature and density, respectively, as a function of filament spine distance. The points are the peaks of the log-normal distribution in filament distance bins, and the error bars show the 68% confidence intervals of individual spines. The pink symbols show the gas properties of the high-luminosity overdensity sample, which traces the hottest and densest gas. The central 1–2 Mpc region of filaments contains the densest hot gas and is optimal for looking for the strongest observational signal in the WHIM.

The Bisous filament finder is shown as a robust trace of not only galaxies, but intergalactic gas in filaments. The galaxy-based luminosity overdensity correlates well with the hot intergalactic gas in the EAGLE simulation. Specifically, regions with high luminosity overdensity are potential WHIM sites for future observational studies. Bisous, which finds filaments based on galaxies alone, captures intergalactic gas that is 25% of the baryon budget in the local universe; this 25% of local universe gas is missing baryons that are not yet observed.

We summarise other results that are indirectly related to the Bisous–LDF–WHIM connection explored in this thesis as follows. EAGLE particle data was combined with the Bisous visit map. The volumes of particle components

inside filaments were calculated from this data. The filaments are contained within 5% of the total EAGLE volume and contain 53% of the baryon gas in the simulation. The hot intergalactic medium in filaments, but outside of galaxy groups, accounts for approximately 79-87% of all the hot WHIM, a large fraction of the missing baryons. The temperature and density profiles agree with results derived from Planck tSZ and CMB lensing observations (Tanimura et al. 2020) within 1 Mpc central regions of filaments.

The analysis was repeated using the NEXUS+ LSS identifier Cautun et al. (2013) for filament detection. While this is a different methodology for determining the filaments, there was only an approximately 10% difference in detected hot WHIM mass compared to Bisous. Both identifiers are in good agreement; however, Bisous has been more extensively used on observed data.

CHAPTER 5

DISCUSSION AND CONCLUSIONS

In Paper I we showed that galaxies in filaments differ from those outside filaments. The increased environment density is known to affect the properties of galaxies (Dressler 1980); however, in our work we made an effort to look beyond the effects arising from environment density alone. Thus, we show that the filament environment specifically modifies galaxy properties in addition to the increased density.

We find that galaxies in filaments are more likely to be elliptical and less star forming in agreement with the cosmic web detachment model (Aragon Calvo et al. 2019), according to which, primordial tendrils, which feed star-forming gas into the centres of galaxy haloes, are cut off by the turbulent matter flows when galaxies enter filaments. A variety of studies based on different galaxy catalogues and filament finders have found similar reddening and star-formation quenching trends in filaments (e.g Alpaslan et al. 2016; Malavasi et al. 2017; Kraljic et al. 2018). The increase in stellar velocity dispersions in both the elliptical and spiral galaxies suggests an enhanced merger rate in filaments and/or accretion near the spines. Group galaxies may have higher peculiar velocities. Alternatively increased satellite galaxy number densities in filaments may be the cause (Guo et al. 2015).

In the morphological distribution we note a deviation from the increasing elliptical morphology fraction near the outskirts of filaments at distances of 1 to 2 Mpc from spines. The increased spiral fraction at these filament distances is in agreement with the results from Kleiner et al. (2016), who found an increase in HI supplies near filaments. The presence of HI gas may provide fuel for star formation, which in turn delays the trend of an increased elliptical-to-spiral morphology relation towards filament spines at the filament outskirts.

Galaxies in the $-18 > M_r > -20$ mag luminosity range showed weaker filament-based trends. The lower-luminosity sample contains considerably fewer galaxies than the higher-luminosity sample. Thus, while some trends might be present, they are difficult to discern from relatively larger uncertainties. Alternatively, the lower environment density at the locations of these galaxies could mean this population is less affected by filaments. On the other hand, these galaxies could be affected by the filament environment, accompanied by a luminosity increase, which together shifts the galaxies into the brighter sample studied.

In Paper II it was found that the change in properties that was detected for all galaxies in Paper I was, in contrast, not present for BGGs. Poudel et al. (2017), who also studied BGGs in filaments using similarly the SDSS and Bisous filament finder, found filament-based effects, namely that in filaments BGGs are more massive and redder.

Of note is that some refinement of the analysis was made between Papers I and II. The filament sample in Paper I was calculated based on a flux-limited selection of galaxies as opposed to a volume-limited sample. In Paper I, distance-based effects were noted in the filament galaxies and efforts were made to account for their effects. Besides catalogue selection, the Bisous algorithm was applied more flexibly in Paper II than in earlier iterations by implementing a variable radius for the cylinders forming the filamentary structure. On top of that, during filament selection, the focus was on filaments residing in regions with roughly average luminosity densities of the galaxy sample. The refined filament sample led us to the finding that groups in those environments are mostly poor, with the number of group members below five. In contrast, Poudel et al. (2017) addressed richer groups, motivated by the use of dynamical masses for group mass estimation. These differences in analysis and target groups may explain the differences between the results of Paper II and Poudel et al. (2017).

The BGG results agree with studies that attribute change in galaxy properties exclusively to the effects of the local environment (e.g. Yan et al. 2013; Eardley et al. 2015; Brouwer et al. 2016). These studies concluded that all filament-based effects can be attributed to the density enhancement driven by increased galaxy numbers in filaments. However, based on Paper II alone, we are cautious in reaching the same conclusion. Paper I and the theoretical work of other groups (Musso et al. 2018; Kraljic et al. 2019) support the picture of filament-based changes in gas accretion into galaxies and groups, which can modulate the evolution of galaxies in these environments. Additionally, as demonstrated in numerous observational and theoretical studies, the anisotropic filament environment does change galaxy orientation (e.g. Libeskind et al. 2013; Hirv et al. 2017; Ganeshiah Veena et al. 2019) adding weight to the filament–galaxy connection picture. Indeed, a recent study of SDSS with the Discrete Persistent Structures Extractor algorithm showed that group centrals experience quenching effects in filaments similar to those of other galaxies (Winkel et al. 2021). In light of our results, we note that different galaxy populations seem to be affected to different extents by the filament, and this aspect of the filament–galaxy connection is worthy of further study.

For a future outlook, further insight can be gained from extending this study to satellite galaxies and isolated galaxies, which were both excluded in the BGG study. In determining the halo masses in observations, more refined methods could be adopted (e.g. HAM methods or machine learning algorithms). While the SDSS has impressive volume–depth balance, its limitations become apparent when looking at the numbers of specific sub-populations of filament galaxies. Additionally, filaments in different large-scale environments are already being targeted in current studies Santiago-Bautista et al. (e.g 2020) that find preprocessing in galaxies falling into clusters along filaments in su-

perclusters. Superclusters are, on average, denser environments compared to the filaments we targeted in Paper II. Likewise, future surveys (i.e. 4MOST, DESI, Euclid, J-PAS) will be helpful for a proper assessment of any weak filament-specific impacts on galaxy properties and for probing weak effects in filaments in a variety of local densities in the large-scale structure.

In Paper III it was shown that the Bisous-determined filaments contain approximately 25% of all baryons in the local universe. At the same time, filaments account for 5% of the total simulation volume, indicating that the Bisous method using galaxy distributions for filament extraction traces the distribution of extragalactic baryonic matter well. Based on the Bisous filaments determined by the locations of galaxies in EAGLE, we confirmed a correlation between luminosity overdensity (defined as $LDF - 1$) at filament spine locations and the WHIM distribution, in agreement with Nevalainen et al. (2015). The galaxy luminosity density field can be used as a trace for the hot WHIM, with higher LDF values correlating with filaments with a high concentration of gas in the hot phase.

The WHIM gas properties we found in EAGLE filaments are in agreement with results from the IllustrisTNG simulation (Galárraga-Espinosa et al. 2021). So far, the study of hot WHIM is restricted to simulations. In order to be able to probe hot WHIM with direct observations, future generations of X-ray observatories are needed (i.e Simionescu et al. 2021).

We can conclude the following main points:

- Tests on simulation data confirm that filaments detected from galaxy distributions with the Bisous algorithm are reliable and trace the underlying diffuse baryonic matter as well.
- The overall galaxy population shows some weak dependence on the distance to filament spines.
- The properties of a clean sample of central galaxies of poor groups appears independent of location with respect to filaments.

REFERENCES

- Alpaslan, M., Grootes, M., Marcum, P. M., et al. 2016, *Galaxy And Mass Assembly (GAMA): stellar mass growth of spiral galaxies in the cosmic web*, MNRAS, 457, 2287
- Alpaslan, M., Robotham, A. S. G., Obreschkow, D., et al. 2014, *Galaxy and Mass Assembly (GAMA): fine filaments of galaxies detected within voids*, MNRAS, 440, L106
- Aragón Calvo, M. A. 2007, *Morphology and Dynamics of the Cosmic Web*, PhD thesis, University of Groningen
- Aragón-Calvo, M. A., Jones, B. J. T., van de Weygaert, R., & van der Hulst, J. M. 2007, *The multiscale morphology filter: identifying and extracting spatial patterns in the galaxy distribution*, A&A, 474, 315
- Aragon Calvo, M. A., Neyrinck, M. C., & Silk, J. 2019, *Galaxy Quenching from Cosmic Web Detachment*, The Open Journal of Astrophysics, 2, 7
- Aragón-Calvo, M. A., van de Weygaert, R., & Jones, B. J. T. 2010, *Multiscale phenomenology of the cosmic web*, MNRAS, 408, 2163
- Baldry, I. K., Balogh, M. L., Bower, R. G., et al. 2006, *Galaxy bimodality versus stellar mass and environment*, MNRAS, 373, 469
- Balogh, M., Eke, V., Miller, C., et al. 2004, *Galaxy ecology: groups and low-density environments in the SDSS and 2dFGRS*, MNRAS, 348, 1355
- Behroozi, P. S., Conroy, C., & Wechsler, R. H. 2010, *A Comprehensive Analysis of Uncertainties Affecting the Stellar Mass-Halo Mass Relation for $0 < z < 4$* , ApJ, 717, 379
- Benítez-Llambay, A., Navarro, J. F., Abadi, M. G., et al. 2013, *Dwarf Galaxies and the Cosmic Web*, ApJ, 763, L41
- Biviano, A., Fadda, D., Durret, F., Edwards, L. O. V., & Marleau, F. 2011, *Spitzer observations of Abell 1763. III. The infrared luminosity function in different supercluster environments*, A&A, 532, A77
- Blanton, M. R., Dalcanton, J., Eisenstein, D., et al. 2001, *The Luminosity Function of Galaxies in SDSS Commissioning Data*, AJ, 121, 2358
- Bond, J. R., Kofman, L., & Pogosyan, D. 1996, *How filaments of galaxies are woven into the cosmic web*, Nature, 380, 603
- Brouwer, M. M., Cacciato, M., Dvornik, A., et al. 2016, *Dependence of GAMA galaxy halo masses on the cosmic web environment from 100 deg² of KiDS weak lensing data*, MNRAS, 462, 4451

- Bruzual, G. & Charlot, S. 2003, *Stellar population synthesis at the resolution of 2003*, MNRAS, 344, 1000
- Camps, P., Trčka, A., Trayford, J., et al. 2018, *Data Release of UV to Submillimeter Broadband Fluxes for Simulated Galaxies from the EAGLE Project*, ApJS, 234, 20
- Catinella, B., Schiminovich, D., Cortese, L., et al. 2013, *The GALEX Arcibo SDSS Survey - VIII. Final data release. The effect of group environment on the gas content of massive galaxies*, MNRAS, 436, 34
- Cautun, M., van de Weygaert, R., & Jones, B. J. T. 2013, *NEXUS: tracing the cosmic web connection*, MNRAS, 429, 1286
- Cautun, M., van de Weygaert, R., Jones, B. J. T., & Frenk, C. S. 2014, *Evolution of the cosmic web*, MNRAS, 441, 2923
- Cen, R. & Ostriker, J. P. 1999, *Where Are the Baryons?*, ApJ, 514, 1
- Chen, Y.-C., Ho, S., Brinkmann, J., et al. 2016, *Cosmic web reconstruction through density ridges: catalogue*, MNRAS, 461, 3896
- Chen, Y.-C., Ho, S., Mandelbaum, R., et al. 2017, *Detecting effects of filaments on galaxy properties in the Sloan Digital Sky Survey III*, MNRAS, 466, 1880
- Codis, S., Pogosyan, D., & Pichon, C. 2018, *On the connectivity of the cosmic web: theory and implications for cosmology and galaxy formation*, MNRAS, 479, 973
- Colberg, J. M., Krughoff, K. S., & Connolly, A. J. 2005, *Intercluster filaments in a Λ CDM Universe*, MNRAS, 359, 272
- Colless, M., Peterson, B. A., Jackson, C., et al. 2003, *The 2dF Galaxy Redshift Survey: Final Data Release*, arXiv e-prints, astro
- Conroy, C., Gunn, J. E., & White, M. 2009, *The Propagation of Uncertainties in Stellar Population Synthesis Modeling. I. The Relevance of Uncertain Aspects of Stellar Evolution and the Initial Mass Function to the Derived Physical Properties of Galaxies*, ApJ, 699, 486
- Conroy, C., Wechsler, R. H., & Kravtsov, A. V. 2006, *Modeling Luminosity-dependent Galaxy Clustering through Cosmic Time*, ApJ, 647, 201
- Cooray, A. & Milosavljević, M. 2005, *What is L_* ? Anatomy of the Galaxy Luminosity Function*, ApJ, 627, L89
- Crain, R. A., Schaye, J., Bower, R. G., et al. 2015, *The EAGLE simulations of galaxy formation: calibration of subgrid physics and model variations*, MNRAS, 450, 1937
- Crone Odekon, M., Hallenbeck, G., Haynes, M. P., et al. 2018, *The Effect of Filaments and Tendrils on the HI Content of Galaxies*, ApJ, 852, 142
- Cui, W., Borgani, S., Dolag, K., Murante, G., & Tornatore, L. 2012, *The effects of baryons on the halo mass function*, MNRAS, 423, 2279

- Danforth, C. W., Keeney, B. A., Tilton, E. M., et al. 2016, *An HST/COS Survey of the Low-redshift Intergalactic Medium. I. Survey, Methodology, and Overall Results*, ApJ, 817, 111
- Darragh Ford, E., Laigle, C., Gozaliasl, G., et al. 2019, *Group connectivity in COSMOS: a tracer of mass assembly history*, MNRAS, 489, 5695
- Darvish, B., Mobasher, B., Martin, D. C., et al. 2017, *Cosmic Web of Galaxies in the COSMOS Field: Public Catalog and Different Quenching for Centrals and Satellites*, ApJ, 837, 16
- Darvish, B., Mobasher, B., Sobral, D., et al. 2015, *Spectroscopic Study of Star-forming Galaxies in Filaments and the Field at $z \sim 0.5$: Evidence for Environmental Dependence of Electron Density*, ApJ, 814, 84
- Darvish, B., Sobral, D., Mobasher, B., et al. 2014, *Cosmic Web and Star Formation Activity in Galaxies at $z \sim 1$* , ApJ, 796, 51
- Davis, M., Efstathiou, G., Frenk, C. S., & White, S. D. M. 1985, *The evolution of large-scale structure in a universe dominated by cold dark matter*, ApJ, 292, 371
- Dekel, A., Birnboim, Y., Engel, G., et al. 2009, *Cold streams in early massive hot haloes as the main mode of galaxy formation*, Nature, 457, 451
- Dolag, K., Borgani, S., Murante, G., & Springel, V. 2009, *Substructures in hydrodynamical cluster simulations*, MNRAS, 399, 497
- Doroshkevich, A. G. 1970, *The space structure of perturbations and the origin of rotation of galaxies in the theory of fluctuation.*, Astrofizika, 6, 581
- Dressler, A. 1980, *Galaxy morphology in rich clusters - Implications for the formation and evolution of galaxies*, ApJ, 236, 351
- Driver, S. P., Hill, D. T., Kelvin, L. S., et al. 2011, *Galaxy and Mass Assembly (GAMA): survey diagnostics and core data release*, MNRAS, 413, 971
- Eardley, E., Peacock, J. A., McNaught-Roberts, T., et al. 2015, *Galaxy And Mass Assembly (GAMA): the galaxy luminosity function within the cosmic web*, MNRAS, 448, 3665
- Ebeling, H., Barrett, E., & Donovan, D. 2004, *Discovery of a Large-Scale Filament Connected to the Massive Galaxy Cluster MACS J0717.5+3745 at $z=0.551$.*, ApJ, 609, L49
- Einasto, J., Suhhonenko, I., Liivamägi, L. J., & Einasto, M. 2018, *Extended percolation analysis of the cosmic web*, A&A, 616, A141
- Einasto, M., Liivamägi, L. J., Tempel, E., et al. 2011, *The Sloan Great Wall. Morphology and Galaxy Content*, ApJ, 736, 51
- Einasto, M., Liivamägi, L. J., Tempel, E., et al. 2012, *Multimodality of rich clusters from the SDSS DR8 within the supercluster-void network*, A&A, 542, A36

- Fadda, D., Biviano, A., Marleau, F. R., Storrie-Lombardi, L. J., & Durret, F. 2008, *Starburst Galaxies in Cluster-feeding Filaments Unveiled by Spitzer*, ApJ, 672, L9
- Frenk, C. S. & White, S. D. M. 2012, *Dark matter and cosmic structure*, Annalen der Physik, 524, 507
- Fukugita, M. & Peebles, P. J. E. 2004, *The Cosmic Energy Inventory*, ApJ, 616, 643
- Galárraga-Espinosa, D., Aghanim, N., Langer, M., & Tanimura, H. 2021, *Properties of gas phases around cosmic filaments at $z = 0$ in the IllustrisTNG simulation*, A&A, 649, A117
- Ganeshaiiah Veena, P., Cautun, M., Tempel, E., van de Weygaert, R., & Frenk, C. S. 2019, *The Cosmic Ballet II: spin alignment of galaxies and haloes with large-scale filaments in the EAGLE simulation*, MNRAS, 487, 1607
- Ganeshaiiah Veena, P., Cautun, M., van de Weygaert, R., et al. 2018, *The Cosmic Ballet: spin and shape alignments of haloes in the cosmic web*, MNRAS, 481, 414
- Giovanelli, R., Haynes, M. P., & Chincarini, G. L. 1986, *Morphological segregation in the Pisces-Perseus supercluster*, ApJ, 300, 77
- Goh, T., Primack, J., Lee, C. T., et al. 2019, *Dark matter halo properties versus local density and cosmic web location*, MNRAS, 483, 2101
- Gómez, P. L., Nichol, R. C., Miller, C. J., et al. 2003, *Galaxy Star Formation as a Function of Environment in the Early Data Release of the Sloan Digital Sky Survey*, ApJ, 584, 210
- Gorgas, J., Cardiel, N., Pedraz, S., & González, J. J. 1999, *Empirical calibration of the lambda 4000 Å break*, A&AS, 139, 29
- Gramann, M. 1993, *An improved reconstruction method for cosmological density fields*, ApJ, 405, 449
- Gunn, J. E. & Gott, J. Richard, I. 1972, *On the Infall of Matter Into Clusters of Galaxies and Some Effects on Their Evolution*, ApJ, 176, 1
- Guo, Q., Tempel, E., & Libeskind, N. I. 2015, *Galaxies in Filaments have More Satellites: The Influence of the Cosmic Web on the Satellite Luminosity Function in the SDSS*, ApJ, 800, 112
- Hahn, O., Porciani, C., Carollo, C. M., & Dekel, A. 2007, *Properties of dark matter haloes in clusters, filaments, sheets and voids*, MNRAS, 375, 489
- Hansen, S. M., Sheldon, E. S., Wechsler, R. H., & Koester, B. P. 2009, *The Galaxy Content of SDSS Clusters and Groups*, ApJ, 699, 1333
- Hearin, A. P., Behroozi, P. S., & van den Bosch, F. C. 2016, *On the physical origin of galactic conformity*, MNRAS, 461, 2135
- Hirv, A., Pelt, J., Saar, E., et al. 2017, *Alignment of galaxies relative to their local environment in SDSS-DR8*, A&A, 599, A31

- Hubble, E. & Humason, M. L. 1931, *The Velocity-Distance Relation among Extra-Galactic Nebulae*, ApJ, 74, 43
- Huchra, J., Jarrett, T., Skrutskie, M., et al. 2005, *The 2MASS Redshift Survey and Low Galactic Latitude Large-Scale Structure*, in *Astronomical Society of the Pacific Conference Series*, Vol. 329, *Nearby Large-Scale Structures and the Zone of Avoidance*, ed. A. P. Fairall & P. A. Woudt, 135
- Huertas-Company, M., Aguerri, J. A. L., Bernardi, M., Mei, S., & Sánchez Almeida, J. 2011, *Revisiting the Hubble sequence in the SDSS DR7 spectroscopic sample: a publicly available Bayesian automated classification*, A&A, 525, A157
- Hwang, J.-S., Park, C., Banerjee, A., & Hwang, H. S. 2018, *Evolution of Late-type Galaxies in a Cluster Environment: Effects of High-speed Multiple Encounters with Early-type Galaxies*, ApJ, 856, 160
- Jõeveer, M. & Einasto, J. 1978, *Has the universe the cell structure*, in *IAU Symposium*, Vol. 79, *Large Scale Structures in the Universe*, ed. M. S. Longair & J. Einasto, 241
- Jones, B. & van de Weygaert, R. 2009, *Cosmic Order out of Primordial Chaos: a tribute to Nikos Voglis*, *Astrophysics and Space Science Proceedings*, 8, 467
- Jones, B. J. T., van de Weygaert, R., & Aragón-Calvo, M. A. 2010, *Fossil evidence for spin alignment of Sloan Digital Sky Survey galaxies in filaments*, MNRAS, 408, 897
- Kaiser, N. 1984, *On the spatial correlations of Abell clusters.*, ApJ, 284, L9
- Kauffmann, G., Heckman, T. M., White, S. D. M., et al. 2003, *The dependence of star formation history and internal structure on stellar mass for 10^5 low-redshift galaxies*, MNRAS, 341, 54
- Kauffmann, G., Li, C., Zhang, W., & Weinmann, S. 2013, *A re-examination of galactic conformity and a comparison with semi-analytic models of galaxy formation*, MNRAS, 430, 1447
- Kauffmann, G., White, S. D. M., Heckman, T. M., et al. 2004, *The environmental dependence of the relations between stellar mass, structure, star formation and nuclear activity in galaxies*, MNRAS, 353, 713
- Kennicutt, Robert C., J. 1998, *Star Formation in Galaxies Along the Hubble Sequence*, ARA&A, 36, 189
- Kereš, D., Katz, N., Weinberg, D. H., & Davé, R. 2005, *How do galaxies get their gas?*, MNRAS, 363, 2
- Kleiner, D., Pimblet, K. A., Heath Jones, D., Koribalski, B. S., & Serra, P. 2016, *Evidence for HI replenishment in massive galaxies through gas accretion from the cosmic web*, MNRAS
- Kraljic, K., Arnouts, S., Pichon, C., et al. 2018, *Galaxy evolution in the metric of the cosmic web*, MNRAS, 474, 547

- Kraljic, K., Pichon, C., Codis, S., et al. 2020, *The impact of the connectivity of the cosmic web on the physical properties of galaxies at its nodes*, MNRAS, 491, 4294
- Kraljic, K., Pichon, C., Dubois, Y., et al. 2019, *Galaxies flowing in the oriented saddle frame of the cosmic web*, MNRAS, 483, 3227
- Kravtsov, A. V., Berlind, A. A., Wechsler, R. H., et al. 2004, *The Dark Side of the Halo Occupation Distribution*, ApJ, 609, 35
- Laigle, C., Pichon, C., Arnouts, S., et al. 2018, *COSMOS2015 photometric redshifts probe the impact of filaments on galaxy properties*, MNRAS, 474, 5437
- Lange, J. U., van den Bosch, F. C., Hearin, A., et al. 2018, *Brightest galaxies as halo centre tracers in SDSS DR7*, MNRAS, 473, 2830
- Li, Y.-T. & Chen, L.-W. 2019, *First ranked galaxies of non-elliptical morphology*, MNRAS, 482, 4084
- Libeskind, N. I., Hoffman, Y., Steinmetz, M., et al. 2013, *Cosmic Vorticity and the Origin Halo Spins*, ApJ, 766, L15
- Libeskind, N. I., van de Weygaert, R., Cautun, M., et al. 2018, *Tracing the cosmic web*, MNRAS, 473, 1195
- Lietzen, H., Tempel, E., Heinämäki, P., et al. 2012, *Environments of galaxies in groups within the supercluster-void network*, A&A, 545, A104
- Liivamägi, L. J., Tempel, E., & Saar, E. 2012, *SDSS DR7 superclusters. The catalogues*, A&A, 539, A80
- Lintott, C., Schawinski, K., Bamford, S., et al. 2011, *Galaxy Zoo 1: data release of morphological classifications for nearly 900 000 galaxies*, MNRAS, 410, 166
- Luparello, H. E., Lares, M., Paz, D., et al. 2015, *Brightest group galaxies and the large-scale environment*, MNRAS, 448, 1483
- Malavasi, N., Arnouts, S., Vibert, D., et al. 2017, *The VIMOS Public Extragalactic Redshift Survey (VIPERS): galaxy segregation inside filaments at $z \simeq 0.7$* , MNRAS, 465, 3817
- Martizzi, D., Vogelsberger, M., Artale, M. C., et al. 2019, *Baryons in the Cosmic Web of IllustrisTNG - I: gas in knots, filaments, sheets, and voids*, MNRAS, 486, 3766
- McAlpine, S., Helly, J. C., Schaller, M., et al. 2016, *The EAGLE simulations of galaxy formation: Public release of halo and galaxy catalogues*, Astronomy and Computing, 15, 72
- Moore, B., Katz, N., Lake, G., Dressler, A., & Oemler, A. 1996, *Galaxy harassment and the evolution of clusters of galaxies*, Nature, 379, 613
- Muru, M. M. & Tempel, E. 2021, *Assessing the reliability of the Bisous filament finder*, arXiv e-prints, arXiv:2103.06619

- Musso, M., Cadiou, C., Pichon, C., et al. 2018, *How does the cosmic web impact assembly bias?*, MNRAS, 476, 4877
- Nevalainen, J., Tempel, E., Liivamägi, L. J., et al. 2015, *Missing baryons traced by the galaxy luminosity density in large-scale WHIM filaments*, A&A, 583, A142
- Oemler, Augustus, J. 1974, *The Systematic Properties of Clusters of Galaxies. Photometry of 15 Clusters*, ApJ, 194, 1
- Park, C., Choi, Y.-Y., Vogeley, M. S., et al. 2007, *Environmental Dependence of Properties of Galaxies in the Sloan Digital Sky Survey*, ApJ, 658, 898
- Peebles, P. J. E. 1969, *Origin of the Angular Momentum of Galaxies*, ApJ, 155, 393
- Peebles, P. J. E. 1980, *The large-scale structure of the universe* (Princeton University Press)
- Peng, Y.-j., Lilly, S. J., Kovač, K., et al. 2010, *Mass and Environment as Drivers of Galaxy Evolution in SDSS and zCOSMOS and the Origin of the Schechter Function*, ApJ, 721, 193
- Pichon, C., Pogosyan, D., Kimm, T., et al. 2011, *Rigging dark haloes: why is hierarchical galaxy formation consistent with the inside-out build-up of thin discs?*, MNRAS, 418, 2493
- Planck Collaboration, Aghanim, N., Akrami, Y., et al. 2020, *Planck 2018 results. I. Overview and the cosmological legacy of Planck*, A&A, 641, A1
- Porter, S. C. & Raychaudhury, S. 2005, *The Pisces-Cetus supercluster: a remarkable filament of galaxies in the 2dF Galaxy Redshift and Sloan Digital Sky surveys*, MNRAS, 364, 1387
- Postman, M. & Geller, M. J. 1984, *The morphology-density relation - The group connection.*, ApJ, 281, 95
- Poudel, A., Heinämäki, P., Tempel, E., et al. 2017, *The effect of cosmic web filaments on the properties of groups and their central galaxies*, A&A, 597, A86
- Rost, A., Stasyszyn, F., Pereyra, L., & Martínez, H. J. 2019, *A comparison of cosmological filaments catalogues*, arXiv e-prints, arXiv:1911.08545
- Salerno, J. M., Martínez, H. J., & Muriel, H. 2019, *Filaments in VIPERS: galaxy quenching in the infalling regions of groups*, MNRAS, 484, 2
- Santiago-Bautista, I., Caretta, C. A., Bravo-Alfaro, H., Pointecouteau, E., & Andernach, H. 2020, *Identification of filamentary structures in the environment of superclusters of galaxies in the Local Universe*, A&A, 637, A31
- Schaye, J., Crain, R. A., Bower, R. G., et al. 2015, *The EAGLE project: simulating the evolution and assembly of galaxies and their environments*, MNRAS, 446, 521
- Shen, S., Yang, X., Mo, H., van den Bosch, F., & More, S. 2014, *The Statistical Nature of the Brightest Group Galaxies*, ApJ, 782, 23

- Shim, J., Lee, J., & Hoyle, F. 2015, *An Observational Detection of the Bridge Effect of Void Filaments*, ApJ, 815, 107
- Shull, J. M., Smith, B. D., & Danforth, C. W. 2012, *The Baryon Census in a Multi-phase Intergalactic Medium: 30% of the Baryons May Still be Missing*, ApJ, 759, 23
- Simionescu, A., Ettori, S., Werner, N., et al. 2021, *Voyage through the hidden physics of the cosmic web*, Experimental Astronomy
- Sousbie, T., Pichon, C., & Kawahara, H. 2011, *The persistent cosmic web and its filamentary structure - II. Illustrations*, MNRAS, 414, 384
- Springel, V. 2005, *The cosmological simulation code GADGET-2*, MNRAS, 364, 1105
- Springel, V., White, S. D. M., Jenkins, A., et al. 2005, *Simulations of the formation, evolution and clustering of galaxies and quasars*, Nature, 435, 629
- Springel, V., White, S. D. M., Tormen, G., & Kauffmann, G. 2001, *Populating a cluster of galaxies - I. Results at $[formmu2]z=0$* , MNRAS, 328, 726
- Tanimura, H., Aghanim, N., Bonjean, V., Malavasi, N., & Douspis, M. 2020, *Density and temperature of cosmic-web filaments on scales of tens of megaparsecs*, A&A, 637, A41
- Tempel, E., Guo, Q., Kipper, R., & Libeskind, N. I. 2015, *The alignment of satellite galaxies and cosmic filaments: observations and simulations*, MNRAS, 450, 2727
- Tempel, E. & Libeskind, N. I. 2013, *Galaxy Spin Alignment in Filaments and Sheets: Observational Evidence*, ApJ, 775, L42
- Tempel, E., Libeskind, N. I., Hoffman, Y., Liivamägi, L. J., & Tamm, A. 2014a, *Orientation of cosmic web filaments with respect to the underlying velocity field*, MNRAS, 437, L11
- Tempel, E., Stoica, R. S., Kipper, R., & Saar, E. 2016, *Bisous model-Detecting filamentary patterns in point processes*, Astronomy and Computing, 16, 17
- Tempel, E., Stoica, R. S., Martínez, V. J., et al. 2014b, *Detecting filamentary pattern in the cosmic web: a catalogue of filaments for the SDSS*, MNRAS, 438, 3465
- Tempel, E., Stoica, R. S., & Saar, E. 2013, *Evidence for spin alignment of spiral and elliptical/S0 galaxies in filaments*, MNRAS, 428, 1827
- Tempel, E. & Tamm, A. 2015, *Galaxy pairs align with Galactic filaments*, A&A, 576, L5
- Tempel, E., Tamm, A., Gramann, M., et al. 2014c, *Flux- and volume-limited groups/clusters for the SDSS galaxies: catalogues and mass estimation*, A&A, 566, A1
- Tempel, E., Tuvikene, T., Kipper, R., & Libeskind, N. I. 2017, *Merging groups and clusters of galaxies from the SDSS data. The catalogue of groups and potentially merging systems*, A&A, 602, A100

- The EAGLE team. 2017, *The EAGLE simulations of galaxy formation: Public release of particle data*, arXiv e-prints, arXiv:1706.09899
- Tilton, E. M., Danforth, C. W., Shull, J. M., & Ross, T. L. 2012, *The Low-redshift Intergalactic Medium as Seen in Archival Legacy HST/STIS and FUSE Data*, ApJ, 759, 112
- Trayford, J. W., Theuns, T., Bower, R. G., et al. 2015, *Colours and luminosities of $z = 0.1$ galaxies in the EAGLE simulation*, MNRAS, 452, 2879
- van de Weygaert, R. & Bond, J. R. 2008, *Observations and Morphology of the Cosmic Web*, in Lecture Notes in Physics, Berlin Springer Verlag, Vol. 740, A Pan-Chromatic View of Clusters of Galaxies and the Large-Scale Structure, ed. M. Plionis, O. López-Cruz, & D. Hughes, 24
- Vogelsberger, M., Marinacci, F., Torrey, P., & Puchwein, E. 2020, *Cosmological simulations of galaxy formation*, Nature Reviews Physics, 2, 42
- Von Der Linden, A., Best, P. N., Kauffmann, G., & White, S. D. M. 2007, *How special are brightest group and cluster galaxies?*, MNRAS, 379, 867
- Weinmann, S. M., van den Bosch, F. C., Yang, X., & Mo, H. J. 2006, *Properties of galaxy groups in the Sloan Digital Sky Survey - I. The dependence of colour, star formation and morphology on halo mass*, MNRAS, 366, 2
- Werner, M. W., Roellig, T. L., Low, F. J., et al. 2004, *The Spitzer Space Telescope Mission*, ApJS, 154, 1
- White, S. D. M. 1984, *Angular momentum growth in protogalaxies*, ApJ, 286, 38
- Winkel, N., Pasquali, A., Kraljic, K., et al. 2021, *The imprint of cosmic web quenching on central galaxies*, MNRAS, 505, 4920
- Yan, H., Fan, Z., & White, S. D. M. 2013, *The dependence of galaxy properties on the large-scale tidal environment*, MNRAS, 430, 3432
- Yang, X., Mo, H. J., & van den Bosch, F. C. 2003, *Constraining galaxy formation and cosmology with the conditional luminosity function of galaxies*, MNRAS, 339, 1057
- York, D. G., Adelman, J., Anderson, Jr., J. E., et al. 2000, *The Sloan Digital Sky Survey: Technical Summary*, AJ, 120, 1579
- Zel'dovich, Y. B. 1970, *Gravitational instability: An approximate theory for large density perturbations.*, A&A, 5, 84
- Zwicky, F. 1933, *Die Rotverschiebung von extragalaktischen Nebeln*, Helvetica Physica Acta, 6, 110
- Zwicky, F. 1938, *On the Clustering of Nebulae*, PASP, 50, 218

SUMMARY IN ESTONIAN

Aine ruumiline paiknemine kõige suuremal mastaabil moodustab võrgutaolise struktuuri. See struktuur koosneb erinevatest elementidest: kõige tihedamalt paikneb galaktikaid võrgustiku sõlmedes olevates galaktikaparvedes, kõige hõredamalt võrgusilmades ehk tühikutes. Vahepealse tihedusega seinad ümbritsevad tühikuid ja filamendid ühendavad sõlmi. Sellist makrostruktuuri kutsutakse kosmiliseks võrgustikuks ja see on tekkinud gravitatsioonilise kokkutõmbumise tõttu ürgsest juhuslikust ainejaotusest. Vaatlusandmetest ja simulatsioonidest on kindlaks määratud, et galaktikate jaotus järgib massivse ent silmale nähtamatu tumeaine jaotust.

Galaktikate parved asuvad sõlmedes, kus galaktikate evolutsiooni mõjutavad nende omavahelised interaktsioonid. Tühikutes arenevad galaktikad peaaegu isolatsioonis. Hõredaid seinu on siiani raske uurida väheste galaktikate arvu tõttu. Filamendid, on ka huvitavad galaktikate keskkonnad, sest siiani ei ole veel täielikult selge kui suurt rolli nad mängivad galaktikate evolutsioonis. Mitmed hiljutised uuringud on proovinud leida vastust just sellele küsimusele.

Teoreetiliste kaalutluste põhjal peaks eeldama, et anisotroopiline ainevool piki filamente muudab galaktikates aine kuhjumist ja tähtede teket. Siiski pole siiani veel kindlaks määratud täpsed filamenti põhised efektid galaktikatele. Kas filamentides asuvad galaktikad kogeavad samasugust ruumilisest ületihedusest tingitud efekte nagu parvedes või on suunatud ainevoolu mõjul veel avastamata füüsikalised protsessid mängus? Selle küsimuse lahendamine täiendab meie arusaamu galaktikate evolutsioonist ja üldiselt meid ümbritseva universumi kohta.

Siinse töö eesmärgiks on leida filamentide mõju galaktikate evolutsioonile ja määratleda selle efekti suurus vaadeldud galaktikates. Selle eesmärgi saavutamiseks kasutasime galaktikate kataloogi kolmemõõtmelise galaktikate asukohtade määratlusega Sloani Digitaalsest Taevaülevalt. Filamentide leidmiseks kasutasime Bisous filamentiotsija algoritmi. Otsitavaks signaaliks on muutused filamentides asuvate galaktikate omadustes. Tähtis on vahet teha filamenti mõjul ja tuntud keskkonna tiheduse mõjul esinevate muutustega. Võrreldes keskkonna mõjuga on filamentidest pärinev signaal väike. Seetõttu on analüüsi käigus olnud tähtis leida tasakaal valimis olevate galaktikate arvu ja keskkonna mõjude kontrollitavuse vahel.

Esiteks võtsime vaatluse alla kaks laiahaardelist galaktikate valimit: heledam galaktikate absoluutheledusega -20 magnituudi r -filtris või heledamad ja väiksema heledusega valim heledustega, vahemikus -18 kuni -20 magnituudi. Galaktikate keskkonna mõõteks kasutasime galaktikate heledustiheduse välja. Otsisime galaktikate omaduste muutust funktsioonina fila-

mendi telje kaugusest. Vaatluse alla võtsime galaktikate massid, värvusindeksid, tähetekke kiirused, morfoloogiate suhtarvud ja heldusjaotuse kontsentratsioonid. Pärast kohaliku keskkonna mõju eraldamist leidsime, et elliptiliste galaktikate osakaal filmendi telje lähedal kasvab, millega kaasneb ka teiste omaduste muutus: värvindekis punanemine ja tähetekke kiiruse vähenemine. Eraldades galaktikad morfoloogia põhjal elliptilisteks ja spiraalseteks lei-dsmie, et nõrk filamendi mõju muudab eraldi nende galaktikate omadusi. Tulemus viitab tõsiasjale, et filamendi keskkond kiirendab galaktikate evolutsiooni sõltumata keskkonna tiheduse kasvust.

Edasises analüüsis pöörasime tähelepanu galaktikate alampopulatsioonidele ja täiustasime galaktikate keskkonna määramise meetodit. Galaktikate valimi piiritlesime -19 magnituudi ja heledamate galaktikateni, et valimis oleks piisaval arvul galaktikaid suhteliselt laias heledusvahemikus. Heledustihedusvälja kasutasime mitmeti: galaktikate kohaliku keskkonna määramiseks nagu esimeses töös ja ka filamentide keskkonna määramiseks. Filamentide valimi piiritlesime vahepealse keskkonna tiheduse väärtusega valimiks, mis sisaldas suurima arvu usaldusväärseid filamente. Pärast filamentides asuvate galaktikate selektsiooni sai ilmsiks, et neis filamentides on peaaegu kõik galaktikate grupid vaesed, s.t. kuue või vähema liikmesgalaktikaga. Kasutades sama selektsiooniga EAGLE simulatsiooni andmeid määrasime, et heledustihedusvälja asukoht grupi heledaima galaktika asuko-has on kõige paremas korrelatsioonis grupi kogu massiga, nii täheaine kui ka tumeaine massiga. Teiste grupi liikmete ja isoleeritud galaktikate jaoks on heledustihedusväli halvem grupi massi määratleja. Edasine analüüs jätkus grupi heledaimate galaktikate põhjal. Võrdlesime värvusindeksite ja tähetekke kiiruse jaotusi filamendis ja filamendist väljas olevate grupi peagalaktikate vahel. Veapiirides kattusid jaotused kõikide parameetrite jaoks. Järeldasime, et filamendi keskkond mõjutab vähe gruppide peagalaktikaid.

Uurimustöö jätkus simuleeritud andmete põhjal. Eesmärk oli vaadelda galaktikatevahelist gaasi, mida on raske vaadelda selle hõreda jaotuse tõttu. Bisous algoritmiga leidsime filamendid EAGLE simulatsioonis 100 Mpc^3 suurses ruumis. Galaktikate valimi piiritlesime sama arvtiheduseni nagu eelnevas töös vaadeldud valimis, et tagada Bisous algoritmi võrreldavus simulatsiooni ja vaatluste vahel. Simulatsiooni andmetega sai hinnata Bisous efektiivsust filamentide gaasi otsimisel. Bisous meetodiga leitud filamendid katavad 5% kogu simulatsiooni ruumalast. Samas asub nendes filamentides 25% galaktikatevahelise gaasi kogumassist. Seda filamentides asuvat gaasi pole veel suudetud otseselt vaadelda. Simulatsiooni andmete põhjal määrasime, et selle gaasi kõige tihedama ja kõrgema temperatuuriga faasi asukohad korreleeruvad galaktikate heledusjaotuse tihedusega. Tulevastes vaatlusprojektides on kasulik galaktikatevahelise gaasi otsimiseks keskenduda heledamate filamentide galaktikate lähedastele asukohtadele.

Selle uurimistöö tulemusena leidsime, et filamentides olevate galaktikate

omadustes on nõrk sõltuvus filamendi telje kaugusest. Samas vaeste gruppide peagalaktikate jaoks filamendi mõju efektiivselt puudub. Simulatsiooni andmete põhjal näeme, et Bisous algoritm filamentide leidmiseks jälgib usalduslikult ka galaktikatevahelise gaasi jaotust.

ACKNOWLEDGEMENTS

The research presented in this Thesis has been financially supported by the Estonian Research Council grants (IUT26-2, IUT40-2 and PUT1627) and the Centre of Excellence “Dark side of the Universe” (TK133), financed by the European Regional Development Fund.

Throughout the writing of this thesis I have received a large amount of support. Grateful thanks go to my supervisor, Antti. Your guidance and patience made this possible. Thank you for helpful advice in science and in life.

I am thankful to the scientists, students and staff at the Tartu Observatory. Most crucially to the people in the cosmology and galaxy physics group, who have been an inspiration on every step in my academic career.

I would like to thank the Nordic Optical Telescope family for opening for me the world of observational astronomy. I am thankful to Thomas for offering a timely studentship position during the writing of this thesis.

I want to give big thanks to fellow students, present and past. Rain, Jaan, Jussi, Toni, Maarja, Punya and Daniel to name just a few. All the difficulties in this endeavour would be worth your friendship alone.

Special thanks go to my parents, Rainer and Riina. Your support sparked in me the curiosity to go so far.

Most of all I am very thankful to my partner Nisa. You were with me to enjoy together during the good times and for encouraging me onward during the bad times. Thank you for being patient and supporting over the years. Last but not least, thank you for our wonderful daughter.

PUBLICATIONS

CURRICULUM VITAE

Personal data

Name	Teet Kuutma
Date and place of birth	21 January 1987, Valga, Estonia
Citizenship	Estonian
Current employment	Tartu Observatory (engineer)
Address	Tartu University Tartu Observatory 61602 Tõravere Tartumaa, Estonia
Phone	(+372) 5688 1373
E-mail	teet.kuutma@ut.ee

Education

1994 – 2006	Valga Gymnasium
2006 – 2010	University of Tartu, undergraduate student, BSc 2010 (physics)
2010 – 2012	University of Tartu, graduate student, MSc 2012 (physics)
2013 – 2021	University of Tartu, PhD student

Employment

2011 – 2013	Tartu Observatory, engineer
2013 – 2014	Tartu Observatory, junior researcher
2014 – 2016	Nordic Optical Telescope, student support astronomer
2016 – 2017	Tartu Observatory, junior researcher
2018 – 2020	Tartu Observatory, University of Tartu, junior research fellow
2020 – 2021	Nordic Optical Telescope, student support astronomer
2021 – ...	University of Tartu, Tartu Observatory, engineer

Professional training

28.07 - 11.08 2012	Summer school "Observational Stellar Astrophysics in the Era of Gaia and Kepler Space Missions", Molėtai, Lithuania
--------------------	--

07.01 - 18.01 2013	Winter school "Nordita Winter School 2013 in High-Energy Astrophysics", Stockholm, Sweden
30.06 – 09.07 2014	Summer school “CSC Summer School in High-performance computing”, Nuukio, Finland.
24.08 – 28.08 2014	Summer school “3rd Scientific Writing for Young Astronomers”, Tihany, Hungary
18.09 - 22.09 2017	Summer school "Cosmology School in the Canary Islands", Fuerteventura, Spain

Conference presentations

21.09 – 22.09 2011	Conference "Tartu - Tuorla annual meeting 2011: Remote sensing of the Universe" Tartu, Estonia. <i>Oral presentation:</i> “Analysis of Galaxy Group Members Colour Index Profiles”
20.09 – 21.09 2012	Conference "Tartu - Tuorla annual meeting 2012: Dark and Visible Universe" Turku, Finland <i>Oral presentation:</i> “Colour and stellar population gradients of galaxies in poor groups of galaxies.”
25.09 - 27.09 2013	Conference "Tartu - Tuorla cosmology conference 2013: Various structures in the Universe", Tõrva, Estonia <i>Oral presentation:</i> "Dust Distribution in Nearby Galaxies"
23.06 – 28.06 2014	Conference “IAU 308: The Zeldovich Universe”, Tallinn, Estonia. <i>Poster presentation:</i> “Structural Decomposition of Galaxies in the CALIFA survey”
07.03 - 08.03 2017	Conference "FMTDK Teaduskonverents 2017", Tartu, Estonia <i>Poster presentation:</i> “From Voids to Filaments: Environmental Transformations of Galaxies in the SDSS”

Language skills

Estonian	the first language
English	very good
Spanish	lower-mid level
German	basic

Honours and Awards

2018

E. Öpik stipend (Tartu Observatory)

Fields of research

Large scale structure of the universe,
galaxy evolution in cosmic filaments.

Publications

1. Tuominen, T., Nevalainen, J., Tempel, E., Kuutma, T., Wijers, N., Schaye, J., Heinämäki, P., Bonamente, M., & Ganeshaiyah Veena, P. 2021, *An EAGLE view of the missing baryons*, *Astronomy & Astrophysics*, 646, A156
2. Einasto, J., Hütsi, G., Kuutma, T., & Einasto, M. 2020, *Correlation function: biasing and fractal properties of the cosmic web*, *Astronomy & Astrophysics*, 640, A47
3. Kuutma, T., Poudel, A., Einasto, M., Heinämäki, P., Lietzen, H., Tamm, A., & Tempel, E. 2020, *Properties of brightest group galaxies in cosmic web filaments*, *Astronomy & Astrophysics*, 639, A71
4. Reed, M. D., Armbrrecht, E. L., Telting, J. H., Baran, A. S., Østensen, R. H., Blay, P., Kvammen, A., Kuutma, T., Pursimo, T., Ketzer, L., & Jeffery, C. S. 2018, *K2 Campaign 5 observations of pulsating subdwarf B stars: binaries and super-Nyquist frequencies*, *Monthly Notices of the Royal Astronomical Society*, 474(4), 5186–5198
5. Kuutma, T., Tamm, A., & Tempel, E. 2017, *From voids to filaments: environmental transformations of galaxies in the SDSS*, *Astronomy & Astrophysics*, 600, L6
6. Nespral, D., Gandolfi, D., Deeg, H. J., Borsato, L., Fridlund, M. C. V., Barragán, O., Alonso, R., Grziwa, S., Korth, J., Albrecht, S., Cabrera, J., Csizmadia, S., Nowak, G., Kuutma, T., Saario, J., Eigmüller, P., Erikson, A., Guenther, E. W., Hatzes, A. P., Montañés Rodríguez, P., Palle, E., Pätzold, M., Prieto-Arranz, J., Rauer, H., & Sebastian, D. 2017, *Mass determination of K2-19b and K2-19c from radial velocities and transit timing variations*, *Astronomy & Astrophysics*, 601, A128
7. Reed, M. D., Baran, A. S., Østensen, R. H., Telting, J. H., Kern, J. W., Bloemen, S., Blay, P., Pursimo, T., Kuutma, T., Slumstrup, D., Saajasto, M., Nielsen, L. D., Harmanen, J., Winans, A. J., Foster, H. M., & Rowe, L. 2016, *A pulsation analysis of K2 observations of the subdwarf B star PG 1142-037 during Campaign 1: A subsynchronously*

rotating ellipsoidal variable, Monthly Notices of the Royal Astronomical Society, 458(2), 1417–1426

8. Johnson, M. C., Gandolfi, D., Fridlund, M., Csizmadia, S., Endl, M., Cabrera, J., Cochran, W. D., Deeg, H. J., Grziwa, S., Ramírez, I., Hatzes, A. P., Eigmüller, P., Barragán, O., Erikson, A., Guenther, E. W., Korth, J., Kuutma, T., Nespral, D., Pätzold, M., Palle, E., Prieto-Arranz, J., Rauer, H., & Saario, J. 2016, *Two Hot Jupiters from K2 Campaign 4*, The Astronomical Journal, 151(6), 171
9. Grziwa, S., Gandolfi, D., Csizmadia, S., Fridlund, M., Parviainen, H., Deeg, H. J., Cabrera, J., Djupvik, A. A., Albrecht, S., Palle, E. B., Pätzold, M., Béjar, V. J. S., Prieto-Arranz, J., Eigmüller, P., Erikson, A., Fynbo, J. P. U., Guenther, E. W., Hatzes, A. P., Kiilerich, A., Korth, J., Kuutma, T., Montañés-Rodríguez, P., Nespral, D., Nowak, G., Rauer, H., Saario, J., Sebastian, D., & Slumstrup, D. 2016, *K2-31B, a Grazing Transiting Hot Jupiter on a 1.26-day Orbit around a Bright G7V Star*, The Astronomical Journal, 152(5), 132
10. Bachulski, S., Baran, A. S., Jeffery, C. S., Østensen, R. H., Reed, M. D., Teltng, J. H., & Kuutma, T. 2016, *Mode Identification in a Pulsating Subdwarf B Star EPIC 212707862 Observed with K2*, Acta Astronomica, 66(4), 455–467
11. Kuutma, T., Tamm, A. & Tempel, E. 2016, *Structural decomposition of galaxies in the CALIFA survey*, Proceedings of the International Astronomical Union, (467-468)
12. Vennik, J. and Kuutma, T. 2013, *Colour and stellar population gradients of galaxies in poor groups of galaxies*, In Wong, T. and Ott, J., editors, Molecular Gas, Dust, and Star Formation in Galaxies, volume 292, pages 164–164

ELULOOKIRJELDUS

Isikuandmed

Nimi	Teet Kuutma
Sünniaeg ja +koht	21 Jaanuar 1987, Valga, Eesti
Kodakondsus	eesti
Praegune töökoht	Tartu Observatoorium (insener)
Aadress	Tartu Ülikooli Tartu Observatoorium 61602 Tõravere Tartumaa, Eesti
Telefon	(+372) 5688 1373
E-mail	teet.kuutma@ut.ee

Haridus

1994 – 2006	Valga Gümnaasium
2006 – 2010	Tartu Ülikool, üliõpilane, BSc 2010 (füüsika)
2010 – 2012	Tartu Ülikool, magistrant, MSc 2012 (füüsika)
2013 – 2021	Tartu Ülikool, doktorant

Teenistuskäik

2011 – 2013	Tartu Observatoorium, insener
2013 – 2014	Tartu Observatoorium, nooremteadur
2014 – 2016	Nordic Optical Telescope, tudeng-tugi-astronoom
2016 – 2017	Tartu Observatoorium, nooremteadur
2018 – 2020	Tartu Ülikool, Tartu observatoorium, nooremteadur
2020 – 2021	Nordic Optical Telescope, tudeng-tugi-astronoom
2021 – ...	Tartu Ülikool, Tartu observatoorium, insener

Täiendkoolitus

28.07 - 11.08 2012	Suvekool "Observational Stellar Astrophysics in the Era of Gaia and Kepler Space Missions", Molétai, Leedu
07.01 - 18.01 2013	Talvekool "Nordita Winter School 2013 in High-Energy Astrophysics", Stockholm, Rootsi
30.06 – 09.07 2014	Suvekool "CSC Summer School in High-performance computing", Nuuksio, Soome.
24.08 – 28.08 2014	Suvekool "3rd Scientific Writing for Young Astronomers", Tihany, Ungari

18.09 - 22.09 2017 Suvekool "Cosmology School in
the Canary Islands",
Fuerteventura, Hispaania

Konverentside ettekanded

21.09 – 22.09 2011 Konverents "Tartu - Tuorla annual meeting 2011:
Remote sensing of the Universe" Tartu, Eesti.
Suuline ettekanne: "Analysis of Galaxy Group
Members Colour Index Profiles"

20.09 – 21.09 2012 Konverents "Tartu - Tuorla annual meeting 2012:
Dark and Visible Universe" Turku, Soome
Suuline ettekanne: "Colour and stellar population
gradients of galaxies in poor groups of galaxies."

25.09 - 27.09 2013 Konverents "Tartu-Tuorla cosmology conference
2013: Various structures in the Universe", Tõrva, Eesti
Suuline ettekanne: "Dust Distribution in
Nearby Galaxies"

23.06 – 28.06 2014 Konverents "IAU 308: The Zeldovich Universe",
Tallinn, Eesti.
Poster: "Structural Decomposition of Galaxies
in the CALIFA survey"

07.03 - 08.03 2017 Konverents "FMTDK Teaduskonverents 2017",
Tartu, Eesti
Poster: "From Voids to Filaments:
Environmental Transformations of Galaxies
in the SDSS"

Keelteoskus

eesti keel	emakeel
inglise keel	väga hea
hispaania keel	madal kesktase
saksa keel	algaja

Autasud ja stipendiumid

2018 E. Öpik stipendium (Tartu Observatoorium)

Peamised uurimissuunad

Universumi suuremastaabiline struktuur,
galaktikate evolutsioon kosmilistes filamentides.

DISSERTATIONES ASTRONOMIAE UNIVERSITATIS TARTUENSIS

1. **Tõnu Viik.** Numerical realizations of analytical methods in theory of radiative transfer. Tartu, 1991.
2. **Enn Saar.** Geometry of the large scale structure of the Universe. Tartu, 1991.
3. **Maret Einasto.** Morphological and luminosity segregation of galaxies. Tartu, 1991.
4. **Urmas Haud.** Dark Matter in galaxies. Tartu, 1991.
5. **Eugene A. Ustinov.** Inverse problems of radiative transfer in sounding of planetary atmospheres. Tartu, 1992.
6. **Peeter Tenjes.** Models of regular galaxies. Tartu, 1993.
7. **Ivar Suisalu.** Simulation of the evolution of large scale structure elements with adaptive multigrid method. Tartu, 1995.
8. **Teimuraz Shvelidze.** Automated quantitative spectral classification of stars by means of objective prism spectra: the method and applications. Tartu, 1999.
9. **Jelena Gerškevič.** Formation and evolution of binary systems with compact objects. Tartu, 2002.
10. **Ivan Suhhonenko.** Large-scale motions in the universe. Tartu, 2003.
11. **Antti Tamm.** Structure of distant disk galaxies. Tartu, 2006.
12. **Vladislav-Veniamin Pustynski.** Modeling the reflection effect in pre-cataclysmic binary systems. Tartu, 2007.
13. **Anna Aret.** Evolutionary separation of mercury isotopes in atmospheres of chemically peculiar stars. Tartu, 2009.
14. **Mari Burmeister.** Characteristics of the hot components of symbiotic stars. Tartu, 2010.
15. **Elmo Tempel.** Tracing galaxy evolution by their present-day luminosity function. Tartu, 2011.
16. **Anti Hirv.** Estimation of time delays from light curves of gravitationally lensed quasars. Tartu, 2011.
17. **Rain Kipper.** Galaxy modelling: dynamical methods and applications. Tartu, 2016, 134 p.
18. **Lauri Juhan Liivamägi.** Properties and spatial distribution of galaxy superclusters. Tartu, 2017, 185 p.
19. **Jaan Laur.** Variability survey of massive stars in Milky Way star clusters. Tartu, 2017, 183 p.
20. **Boris Zhivkov Deshev.** On the coevolution of galaxies and their host clusters. Tartu, 2019, 199 p.
21. **Tiina Liimets.** Nebulosities and jets from outbursting evolved stars. Tartu, 2019, 207 p.
22. **Maarja Bussov.** Clustering Analysis for Astrophysical Structures. Tartu, 2020, 113 p.